Bulletin of Geophysics and Oceanography Vol. XX, n. X, pp. XXX-XXX; Xxxxx 20xx
DOI 10.4430/bgo00542

Last glacial and deglaciation dynamics of the ice sheet and valley glaciers in the northern Drygalski Basin off northern Victoria Land (Antarctica)

C. Sauli[1], M. Busetti[1], L. De Santis[1], R. Melis[2], R. Tolotti[3], E. Colizza[2], L. Baradello[1], G. Brancatelli[1], D. Accettella[1], M. Caffau[1], R. Romeo[1], M. Burca[1], N. Corradi[3], D. Morelli[3] and A. Caburlotto[1]

[1] *National Institute of Oceanography and Applied Geophysics - OGS, Trieste, Italy*
[2] *Department of Mathematics, Informatics and Geosciences, University of Trieste, Trieste, Italy*
[3] *Department of Earth, Environmental and Life Sciences, University of Genova, Genova, Italy*

(Received: 6 November 2025; accepted: 28 July 2026; published online: 12 November 2026)

ABSTRACT Glaciers crossing the Transantarctic Mountains and flowing from the coastal areas of Victoria Land, together with the Antarctic ice sheet (AIS) extending to the continental shelf, contributed to filling the westernmost basins of the Ross Sea and shaping their morphobathymetry, up to the last glacial period. The objective of this work is to investigate evidence of glacial dynamics in the northern Drygalski Basin, including the incursion, asynchronous interactions, and stationing of both large ice streams draining the AIS and outlet or valley glaciers from Victoria Land. Since at least the Last Glacial Maximum (26.5 to 19–20 ka), the Borchgrevink and Mariner glaciers of northern Victoria Land expanded and carved the valley between the coast and Coulman Island. Their retreat to their present-day positions was not linear as indicated by geomorphological features that characterise the Borchgrevink Coast grounding zone wedge complex, investigated here for the first time using morphobathymetric and seismic-acoustic data combined with sediment cores.

Key words: western Ross Sea, northern Drygalski Basin, grounding zone wedge, grounding line embayment, glacial bedform, glacial sediment facies.

1. Introduction

The grounding line of marine ice sheets is where streaming ice detaches from the seafloor and starts floating, while the ice front represents the terminal margin where the marine ice sheet or ice shelf disintegrates into icebergs (Anderson *et al*., 2002, 2014; Alley *et al*., 2007; Smith *et al*., 2019). Since the 2000s, identifying these past ice boundaries on the Ross Sea continental shelf has been central to mapping ice expansion and retreat during and after glacial maxima (Bentley *et al*., 2014; Halberstadt *et al*., 2016; Lee *et al*., 2017; Spector *et al*., 2017; Prothro *et al*., 2018, 2020; Goehring *et al*., 2019). Analysing depositional geometry, sedimentary facies, and sediment dating has revealed the spatial and temporal patterns of seafloor-anchored ice (and the presence of floating ice) at the Last Glacial Maximum (LGM) (26.5 to 19–20 ka) and during subsequent deglaciation (Shipp *et al*., 1999; Prothro *et al*., 2018, 2020; Danielson and Bart, 2023).

This work aims to reconstruct the grounding and calving dynamics of the Antarctic ice sheet

© 2026 - The Author(s)

(AIS) and the Transantarctic Mountains (TAM) coastal glaciers in the north-western Ross Sea during their LGM expansion and post-LGM retreat.

The shallower and rugged topography of the western Ross Sea, characterised by islands and banks such as Coulman Island and Mawson Bank, provided pinning points for the AIS. As a result, its retreat after the LGM was slower than in the deeper and flatter eastern Ross Sea, leading to the formation of ice grounding zone wedges (GZWs) made of ice proximal sediments, thick enough to be clearly identified and mapped (Shipp *et al*., 1999; Anderson *et al*., 2014; Goehring *et al*., 2019; Robinson *et al*., 2021; Danielson and Bart, 2023).

The northern Drygalski Basin (hereafter nDB) in the north-western Ross Sea was influenced by valley glaciers from northern Victoria Land (NVL) (Lee *et al*., 2017; Spector *et al*., 2017; Goehring *et al*., 2019), by valley and outlet glaciers from southern Victoria Land, including the David Glacier (Greenwood *et al*., 2018) and a large marine-based ice sheet fed by the East AIS (EAIS) and the West AIS [WAIS (Naish *et al*., 2009; Pollard and DeConto, 2009)].

During the LGM, the ice sheet was grounded over the north-western continental shelf, north of Coulman Island forming the Coulman Island GZW (CIGZW) on the western side of the Mawson Bank (Licht *et al*., 1996, 1999; Shipp *et al*., 1999, 2002; Melis *et al*., 2002; Colizza *et al*., 2003; Melis and Salvi, 2009; Prothro *et al*., 2018, 2020; Robinson *et al*., 2021).

After the LGM, the retreat of the ice sheet in the Ross Sea was complex and asynchronous, with deglaciation beginning around 16.4 cal ka BP (Pambianco *et al*., 2025), or later, at 13 cal ka BP (Danielson and Bart, 2024), in the Joint Oceanographic Institutions for Deep Earth Sampling (JOIDES) Basin, and around 16.5 cal ka BP (Anderson *et al*., 2014; Prothro *et al*., 2020) in the Drygalski Basin. Ice streams receded from the troughs and banks, following the 'deglacial emergent' ice rise model proposed by Matsuoka *et al*. (2015), which formed indentations in the basins. The timing, modality and rate of ice sheet retreat from the Drygalski Basin are poorly understood, as post-LGM grounding lines have been reconstructed only near the modern Drygalski Ice Tongue at approximately 11 cal ka BP (Licht *et al*., 1996; Cunningham *et al*., 1999; Domack *et al*., 1999) or inferred at 15 cal ka BP in the southern Drygalski Basin (Prothro *et al*., 2020). Calving lines are close together in the southern Drygalski Basin [10.5 cal ka BP (Domack *et al*., 1999), core NBP 95–01 KC37] and south of Terra Nova Bay [~8.6–7 ka BP (Yokoyama *et al*., 2016)], suggesting the persistence of a broad ice shelf along the coast during the last 10 ka (McKay *et al*., 2008, 2016).

By combining evidence from morphobathymetric bedforms with stratal architecture and sedimentary facies in the nDB, this work aims to address four key unknowns:

i) the behaviour of coastal valley glaciers flowing through the TAM and expanding into the nDB;
ii) the interaction between the AIS and these glaciers;
iii) the influence of the glaciers on the construction of the CIGZW, the stability and permanence of the AIS in the area, and the subsequent formation and persistence of a post-LGM floating ice shelf;
iv) the mode and timing of the last(?) deglaciation, also in comparison with the adjacent, more easterly JOIDES Basin, which was not directly influenced by coastal glaciers.

The scientific relevance of this work lies in providing evidence for the reconstruction of the glacial history of the westernmost Ross Sea, a strategic sector for understanding the interplay between the AIS and the marine-terminating glaciers.

Our results contribute to clarifying factors that regulated past ice stability in this strategic sector. By investigating this 'coastal corner' we provide a crucial field-based constraint for ice–ocean interaction models. As these glaciers of NVL, located near the continental shelf margin, are

among the first to be exposed to oceanic warming, they represent ideal systems for examining ice-ocean interactions in response to past climate forcing, thus helping to constrain models that project future warming scenarios.

2. Regional setting

The study area is in the north-western Ross Sea, within the nDB, in a sector bounded to the south by a morphological sill nearly 100 m high at approximately 73°10' S, and to the east by the Borchgrevink Coast and the area off the Daniell Peninsula (Figs. 1 and 2). The seafloor depth ranges from less than 400 m on morphological banks to 1,000 m in the valley between the coast and Coulman Island (see Fig. 2). The Mesozoic–Cenozoic sedimentary sequence of the basin was deposited within the westernmost rift basins of the Ross Sea , which developed during the Late Cretaceous and Cenozoic tectonic phases of the West Antarctic Rift System (Cooper *et al*., 1987; Brancolini *et al*., 1995; Salvini *et al*., 1997; Sauli *et al*., 2021), and it was subsequently shaped by Neogene–Quaternary glacial activity (Bart *et al*., 2000, 2011; Sauli *et al*., 2014; Pérez *et al*., 2022).

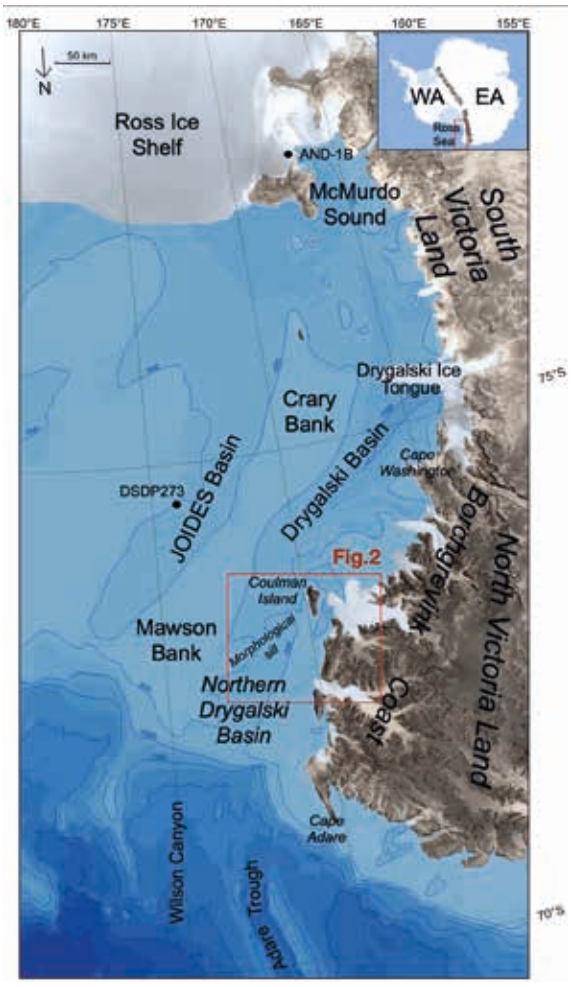


Fig. 1 - Map of the western Ross Sea showing the locations of the JOIDES and Drygalski basins, separated by the Mawson and Crary banks. The study area in the nDB is marked by a red rectangle (see Fig. 2). Bathymetry is from Dorschel *et al.* (2022). All locations mentioned in the text are indicated on the map, including Victoria Land to both the south and north (SVL and NVL), which border the western Ross Sea to the west, as well as the Borchgrevink Coast extending from Cape Washington to Cape Adare, the modern Ross Ice Shelf, the McMurdo Sound area to the south, and Wilson Canyon and Adare Trough to the north. The Drygalski Ice Tongue is shown in the Drygalski Basin, and the morphological sill, where the basin opens onto the outer shelf, is shown in the nDB beyond Coulman Island. The position of drill sites DSDP 273 and AND-1B are displayed. The smaller inset shows Antarctica, with West Antarctica (WA) and East Antarctica (EA) separated by the TAM, the Ross Sea, and the area marked by a red rectangle in Fig. 1.

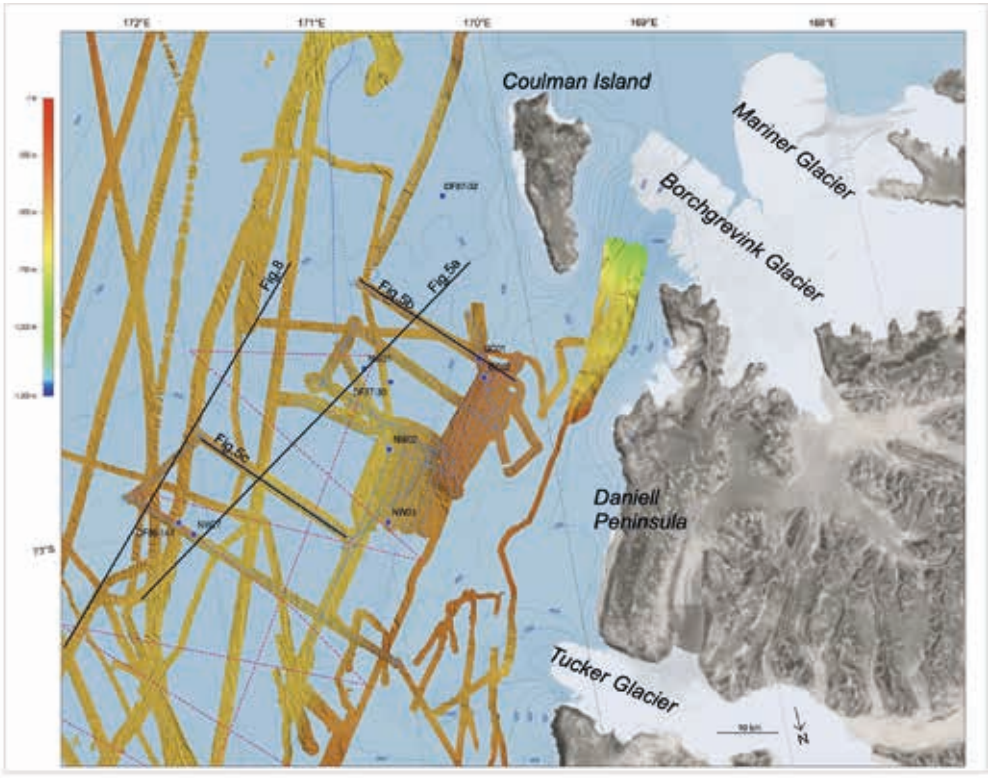


Fig. 2 - Bathymetric map of the nDB, located north of Coulman Island and off the Daniell Peninsula, showing multibeam grids (25 m × 25 m) from PNRA GLEVORS and VILD data, and USAP NBP data. Track lines of sub-bottom profiles (2017 PNRA GLEVORS) and sparker profiles (1998–99 and 2001/02 PNRA projects) are shown as blue and pink lines, respectively. The locations of the Borchgrevink–Mariner glaciers and Tucker Glacier are indicated along the coast. Track lines of multichannel and single-channel seismic profiles shown in Figs. 5 and 8 respectively, are also indicated. The locations of 2017 GLEVORS sediment cores GC01 and GC02, as well as previously published cores, both revised and unrevised in this paper, are shown: 1999 and 2002 PNRA sediment cores NW27, NW30, NW31, NW02, and NW03, and USA 1980 and 1987 sediment cores DF87-30, DF87-32, and DF80-144.

Evidence of the distinctive tectonic and particularly volcanic evolution of the study area is shown by the origin and volcanic composition of Coulman Island and the Daniell Peninsula, which border it to the south and west along the coast, respectively. In this area, several glaciovolcanic sequences of the Late Miocene–Early Pliocene Hallett Volcanic Province outcrop (Smellie and Rocchi, 2021). Additional evidence comes from recent offshore magmatism that has characterised NVL, both in the Adare Basin (Granot *et al*., 2010) and along the Pennell Coast (Civile *et al*., 2025).

The Drygalski Basin was glacially excavated both in its deep southern part, at the mouth of the David Glacier, and in its northern part (which opens onto the outer continental shelf) by the David Glacier and other coastal glaciers originating from the TAM in Victoria Land, and flowing along the Borchgrevink Coast, during the Miocene to early Pleistocene (Sauli *et al*., 2014). As indicated by the biostratigraphic dating of diatoms and the correlation with a coeval sediment section drilled in McMurdo Sound at the AND-1B drill site (Naish *et al*., 2009; Bart *et al*., 2011), the Plio–Quaternary sedimentary infill of the nDB [glacial Unit 9 to Unit 1 (Bart *et al*., 2000, 2011)] may have been deposited during major expansions of the WAIS. The uppermost and youngest Unit 1 and Unit 2 are interpreted as having been deposited during the LGM (Domack *et*

al., 1999; Shipp *et al*., 1999) and pre-LGM periods, respectively. Unit 1 pinches out near Coulman Island while Unit 2 pinches out on the outermost shelf (Bart *et al*., 2000). Neither unit progrades onto the continental slope, unlike underlying Unit 3. Unconformity 2, at the top of pre-LGM Unit 2, is interpreted as the base of the nDB and the base of the JOIDES Basin, and was cored by DSDP 273 on the flank of the JOIDES Basin (Fig. 1) (Bart *et al*., 2000; Bart and Anderson, 2000). Based on their stratal geometries, Unit 1 and Unit 2 were interpreted as recessional deposits resulting from the last WAIS oscillations, while diatom-biostratigraphic dating has shown that only two major advances of grounded ice have occurred since 0.71 Ma (Bart *et al*., 2011).

In the western Ross Sea, the LGM and the post-LGM sequences comprise the following three main subglacial and glaciomarine types of sediments:

i) subglacial diamicton, a matrix of sand, silt, and clay with clasts of variable size. It represents the typical facies resulting from processes occurring at the base of grounding ice (e.g. dragging, remoulding, faulting, meltwater sorting, pore water expulsion due to sediment compaction) [till or facies 1 of Prothro *et al*. (2018, 2020), Smith *et al*. (2019), and Robinson *et al*. (2021)]. In most of the cases, subglacial sediments include older diamicton and marine sediments (Licht *et al*., 1999; Shipp *et al*., 1999, 2002; Robinson *et al*., 2021);

ii) glaciomarine sediments lying in front of the grounding line have facies similar to diamicton, but generally present a certain degree of sediment sorting due to deposition as waterlain till and/or as out-wash meltwater fan inclined forested beds [facies 2 of Prothro *et al*. (2018, 2020)]. Glaciomarine sediments formed from melting of basal debris may include pelletised diamicton [facies 3 of Prothro *et al*. (2018, 2020)]. Stratified diamicton and muddy sediment are interpreted as plumites deposited beneath the ice shelf [facies 4 of Prothro *et al*. (2018, 2020)], representing the transition from glacial to deglacial conditions. These sediments are often interbedded with sandy layers that originated from bottom water reworking in open water. Meltwater plume deposits frequently occur between 10 km and 250 km from the grounding zone. Their characteristic is high water content, low amount of biogenic matter and of ice-rafted debris (IRD) (Simkins *et al*., 2017; Prothro *et al*., 2018, 2020; Majewski *et al*., 2020). With increasing distance from the grounding line and closer proximity to the calving line, the glaciomarine sediments exhibit an enhanced marine signature, characterised by better sorting and stratification, higher IRD, total organic carbon, absolute diatom abundance (ADA), biogenic silica, carbonate and sand content, as well as greater abundance and variability of foraminifera;

iii) a sandy silt is the uppermost unit normally younger than 7 ka, consisting of terrigenous mud enriched in diatoms, and deposited in an increasingly open-marine depositional regime, in which the bottom current removes the fine-grained component (Anderson *et al*., 1991; Domack *et al*., 1999; Licht *et al*., 1999; Mckay *et al*., 2008).

3. Methods

This work is based on geological and geophysical data collected since 1980 by the Italian Antarctic National Program (PNRA) and the United States Antarctic Program (USAP). These data include sediment cores, multibeam data grids, and seismic and acoustic profiles. The legacy data and previous results were integrated with data collected in 2017 by the PNRA Glacial Evolution in the north-western Ross Sea (GLEVORS) project, offshore NVL, such as sediment cores and sub-bottom profiles (Fig. 2).

3.1. Geophysical data

Morphobathymetric data, sub-bottom and sparker profiles, as well as medium- and low-resolution seismic profiles, both single-channel and multichannel, were processed and interpreted to investigate the seafloor morphobathymetry and shallow stratigraphy (see Fig. 2 and Table 1).

Table 1 - Core name, position, and acquisition information for the PNRA-GLEVORS cores.

Core name	Latitude (°S)	Longitude (°W)	Water depth (m)	Length (cm)	Cruise/reference
IT17RS-GC_01	73.21017	170.32383	381	100	GLEVORS Project XXX PNRA 2017 Expedition R/V OGS Explora 2017
IT17RS-GC_02	73.17833	170.31250	358	166	GLEVORS Project XXX PNRA 2017 Expedition R/V OGS Explora 2017

Merged bathymetric grids include data acquired in 2006 and 2017 (from the PNRA VILD and GLEVORS projects, respectively) and the Global Multi-Resolution Topography (GMRT) synthesis, version 3.8 (2020), hosted by the Lamont-Doherty Earth Observatory of Columbia University (Carbotte *et al*., 2007). The GMRT data were downloaded as maximum-resolution grid tiles and outlier removal was applied to the resulting gridded dataset. The three datasets were subsequently combined into a final grid with a uniform cell size of 25 m × 25 m.

High-resolution single-channel seismic data (Fig. 2) include the PNRA GLEVORS (Gi-gun in the Appendix) reflection seismic and sub-bottom chirp profiles, and the 1998/99 PNRA sparker profiles (Corradi *et al*., 2003a, 2003b).

GLEVORS chirp data, stored in full-wave mode, were processed to improve the signal-to-noise ratio using traditional seismic processing methods (Quinn *et al*., 1998; Baradello, 2014; Zhu *et al*., 2016) and additional steps to enhance lateral and vertical resolution.

Qualitative analysis and mapping of glacial and other bedforms were conducted on multibeam grids and sub-bottom profiles used to image the sedimentary geometry and acoustic facies below the seafloor. The analysis, identification, and classification of morphobathymetric features in the multibeam grids were conducted using Global Mapper®, a geographic information system software package developed by Blue Marble Geographics, while the acoustic and seismic profiles were interpreted with the Kingdom™ Geoscience Software by S&P Global.

3.2. Sediment cores

Direct constraints on age and lithological composition of the uppermost and youngest sedimentary sequence are based on previously published sediment cores from PNRA and USAP projects collected since 1996. Kasten and gravity cores collected from the north-western Ross Sea study area include USAP cores DF87-30, DF87-32, and DF80-144 (Licht *et al*., 1996, 1999), as well as PNRA cores ANTA99-NW31, ANTA99-NW27, ANTA02-NW02, and ANTA02-NW03 [hereafter NW31, NW27, NW02, and NW03 (Melis *et al*., 2002; Colizza *et al*., 2003; Del Carlo *et al*., 2015); see Fig. 2 for location].

Moreover, the two sediment gravity cores IT17RS-GC_01 and IT17RS-GC_02 (hereafter GC01

and GC02; see Table 1 for general information), collected in 2017 by the PNRA-GLEVORS project north of Coulman Island (Fig. 2), were also analysed for grain size, water, and micropalaeontological content. Bulk density (gamma ray attenuation) and magnetic susceptibility (MS) were measured using a Geotek® multi-sensor core logger and the cores were X-rayed using Geotek® X-ray core imaging.

The sediment grain size was determined using a laser MALVERN Mastersiser Hydro 2000S for the size fraction smaller than 2 mm. The fraction larger than 2 mm was separated by wet-sieving and counted under an optical microscope. Sand and mud classes were determined following the grain-size classification by Wentworth (1922) while the mean diameter (Mz) was calculated following Folk and Ward (1957).

A total of 11 sediment samples from the GC01 core and 43 from the GC02 core were analysed for calcareous microfossils. The samples prepared were wet-sieved using a 63 µm mesh and the entire fraction larger than 63 µm was examined. Both the planktonic and benthic foraminifera densities were expressed as the number of specimens per gram of total analysed dry sediment (n. specimens/g dry sed.).

A preliminary set of complete smear slides from both cores indicated that the sequences were generally poor in biogenic silica and reworked material. Based on these observations, 15 samples (five from core GC01 and ten from core GC02) were collected and analysed for biogenic silica content in the shallowest layers, according to Schrader and Gersonde (1978), Barde (1981), and Bodén (1991). The diatom counting procedure, performed by means of a light microscope, specifically a Reichert Jung-Polyvar microscope (oil-immersion 1000×, Vienna, Austria), enabled to obtain the quantitative logs (i.e. ADA), expressed in diatom valves per gram of dry sediment (valves g-1 ds), following Warnock and Scherer (2014).

The chronology of these cores is based on seven radiocarbon dates obtained through accelerator mass spectrometry. The uncorrected dates from articles published by Licht *et al*. (1996, 1999), Melis *et al*. (2002), and Colizza *et al*. (2003) have been uniformly recalibrated using the procedure listed in the Appendix, the results of which are reported in Table A2.

4. Results

Geophysical data and sedimentary cores are used to identify and describe glacial landform and bedforms (Figs. 3, 4, 5, 7, 8, and 9 and Table 2) in three sectors of the nDB: along the Borchgrevink Coast off NVL (Section 4.1), north of Coulman Island (Section 4.2), and in the area between them (Section 4.3).

4.1. The Borchgrevink Coast

4.1.1. Geomorphic features and acoustic facies

A marine morphological bank extends along the Borchgrevink Coast, offshore from the Daniell Peninsula, covering an area of 363,690 km² and reaching depths as shallow as 400 m (Figs. 3a and 3b). GLEVORS sub-bottom profiles show that it is asymmetric, with steeper eastern and north-eastern flanks (Fig. 4). The SW part of the inner bank's surface displays parallel, elongated ridges averaging 5 m in height, with locally overlapping ridges and grooves which are oriented ENE–WSW, E–W, and N–S (Figs. 3a and 3b). The NE sector of the bank's surface is incised by deep (20–30 m), randomly distributed furrows (Fig. 3b), as well as numerous, nearly concentric, deep

(20 m), step-like furrows that are north/NE-aligned and parallel to the edge of the bank (Fig. 3b and Table 2).

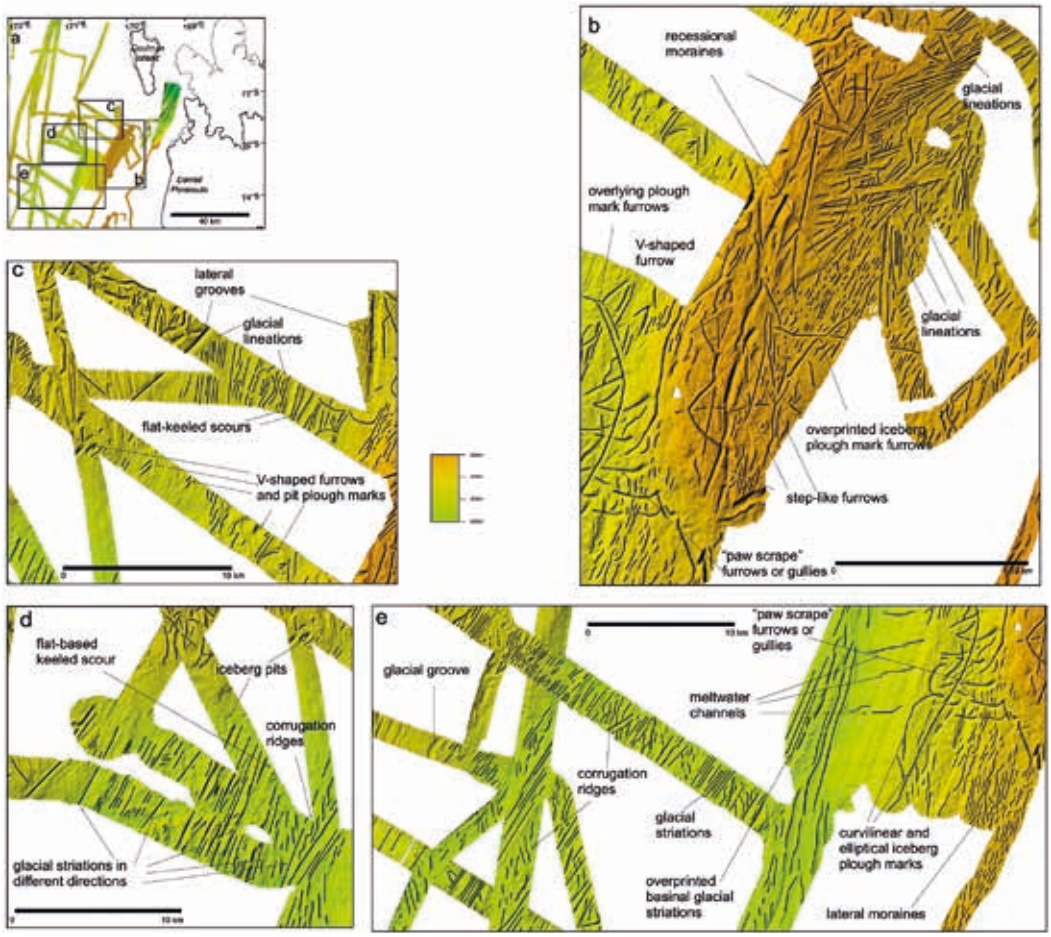


Fig. 3 - Morphobathymetric data. a) Overall view. b) Innermost coastal segment of the Borchgrevink Coast grounding zone wedge complex (BCGZWC). In this zone, distinct generations of elongated sediment ridges, indicative of subglacial formation, are interpreted as mega scale glacial lineations (MSGLs), i.e. the depositional result of carving patterns, produced by the rapidly advancing Borchgrevink and Mariner glaciers, which flowed in the N–S, ENE–WSW, and E–W directions. Recessional moraines, along with palaeo- and modern iceberg plow marks on the BCGZWC surface and in the offshore area of the BCGZWC, are also identified. On the outermost edge of the GZW surface in the north-eastern region, deep, subconcentric, subparallel, slightly stepped furrows are observed (stepped slides or iceberg furrows?). c) Inner part of the southern sector of the nDB. Within the inner basin, which is bordered by lateral grooves, nonparallel, flat-keeled scours overprint nearly N–S-trending glacial lineations (GLs). Conversely, V-shaped and pit plow marks are visible farther north. d) Central sector of the southern nDB between the BCGZWC and the southern CIGZW. Within this zone, continuous, linear, nonparallel, divergent/convergent, overprinted glacial scours are present, with a cluster of predominant NNE–SSW striations within which flat-keeled scours also occur. Some oblique corrugation ridges are observed in the west. e) Outer sector of the southern nDB in front of the northern CIGZW and the north-eastern BCGZWC. Within this zone, from west to east, the following features are highlighted: a cluster of subparallel, curved cuts extending along the slope and nearly perpendicular to the BCGZWC, i.e. 'paw scrapes' (gullies?); overlying iceberg plough marks, tens of kilometres long, curvilinear and elliptical; and meltwater channels extending farther out on the debris lobe. The glacial striations on the western margin of the basin floor appear to diverge from those in the inner basin and are covered by debris-flow material. Within the basin, an ice-shelf keel mélange zone is detectable, and the observed ice-keel furrows show a predominantly NE–SW orientation. The arrangement of features, including linear glacial scours and superimposed subparallel oblique ridge packages, closely resembles a 'washboard' pattern.

Table 2 - Summay of the seafloor glacial features recognised in the study area, their appearance on multibeam data and on sub bottom profiles as well as a brief description.

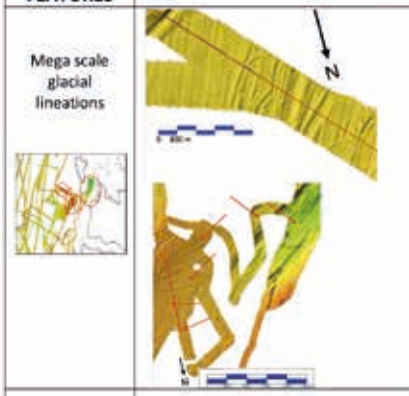
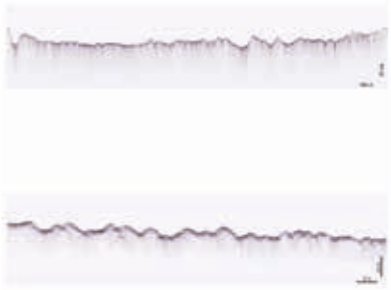
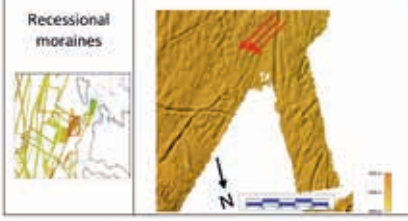
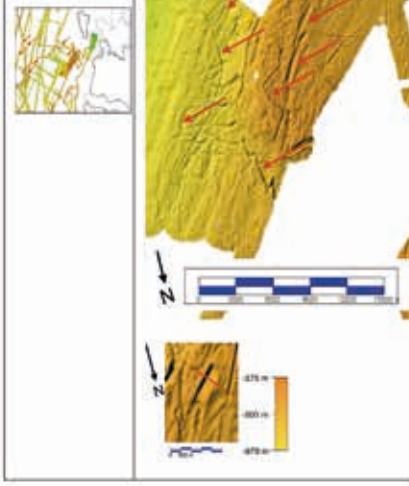
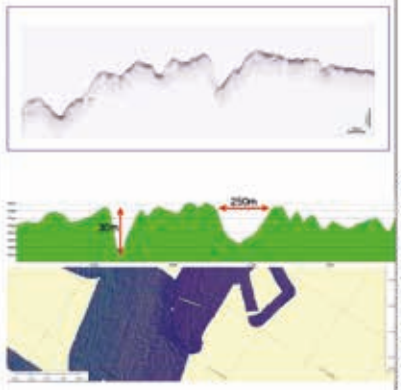
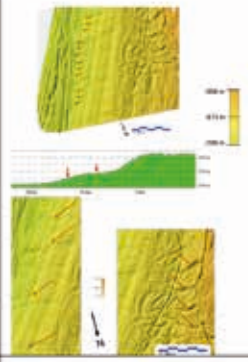
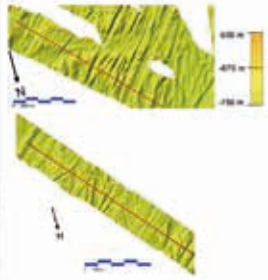
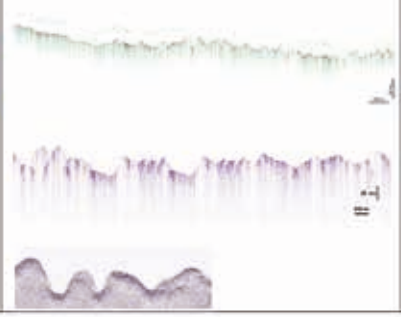
SEAFLOOR GLACIAL FEATURES	MULTIBEAM	SUBBOTTOM PROFILES	DESCRIPTION
Mega scale glacial lineations			Elongate sedimentary features oriented in the direction of regional ice flow form sub glacially in soft sediments due to the carving patterns of advancing ice. References: Spagnolo *et al.*, 2014; Dowdeswell *et al.*, 2016.
Recessional moraines			They form as backstepping sediment deposits from a receding ice sheet or glacier; these transverse ridges indicate the direction and rate of ice retreat. Symmetrical in shape, they are spaced nearly 300 m apart, 15–17 m high, and 300 m long. References: Jakobsson *et al.* 2011; Graham *et al.*, 2013; Dowdeswell *et al.*, 2020.
Iceberg plough marks			Scours caused by iceberg keels have been observed at modern water depths of 400 to 500 m. These scours may be deep or shallow, continuous, linear or arcuate, flat, multi-keeled, or in the form of pits. The elliptical, curvilinear, and spiral marks are inferred to result from iceberg drift influenced by both tidal and geostrophic currents. References: Woodworth-Lynas *et al.* 1991; Dowdeswell *et al.* 2007; MacAyeal *et al.* 2009.

Table 2 - continued.

Claw furrows and meltwater channels on the glacial debris flow cone			The 'paw scrape', i.e. claw furrows, are orientated almost perpendicular to the GZW at the base of the GZW. while the presumed canyons are found further down on the upper flat part of the frontal glacial debris cone. Presumed meltwater canyons are found further down on the upper flat part of the frontal glacial debris cone.
Ice shelf *mélange* scours and 'washboard pattern'			*Mélange* scours result from the scouring action of the keels of calved icebergs, which are pushed forward by the ice shelf and held in place by sea ice. Grounding of iceberg keels, which rotate under the influence of tides, currents, and wind, produces the 'washboard pattern' – an alternation of lineation grooves and fine-scale (approximately 150–12 m in dimension) transverse ridges, known as corrugation ridges. References: Jacobsson *et al.*, 2011; Smith *et al.*, 2019.

Off the north–north-eastern edge of the coastal morphological bank, at the base of its steeper leeward side, a frontal convex cone-like feature dips at an angle of 20–30° towards the north-NE and extends for several tens of kilometres (Figs. 3a, 3e, 4b, and 4c and Table 2). Subparallel curved incisions are observed on the surface of the upper part of the cone-like feature ('paw scrape' furrows), while farther offshore, on the surface of the slightly sloping seaward cone-like feature, channels up to 5 m deep and about 500 m wide are present (see Fig. 3e and Table 2).

The bank on the seismic profiles displays a hummocky, rugged surface with deep (15–30 m) incisions (Figs. 4a and 4b). The acoustic facies at the top and front of the bank consist of eastward-prograding clinoforms that downlap onto an erosional surface, which truncates the underlying subhorizontal strata (Fig. 5). The bank's seafloor is strongly reflective, while the cone-like feature observed in multibeam data off the north–north-eastern edge of the bank (Figs. 4b and 4c) shows up to 5 m of penetration in the deeper area east of the bank, where a package of stratified, parallel, continuous reflectors drapes an undulated subsurface.

4.1.2. GLEVORS sediment core characteristics

Gravity cores GC01 and GC02 were collected: the first from the seaward slope, within a furrow between two seafloor ridges, and the second from the top of the bank, directly on a seafloor ridge (Figs. 2 and 4a).

The sediment of the two cores is mainly composed of diamicton (clast-rich sandy-silty matrix). Two main lithological units (Unit 1 and Unit 2) are distinguished based on geotechnical, physical, and micropalaeontological characteristics (Figs. 4a and 4b).

Unit 1, which represents the oldest part of the cores with an age greater than 20 ka BP, consists of olive-grey diamicton, with >2 mm clasts more concentrated between 15 and 22 cm

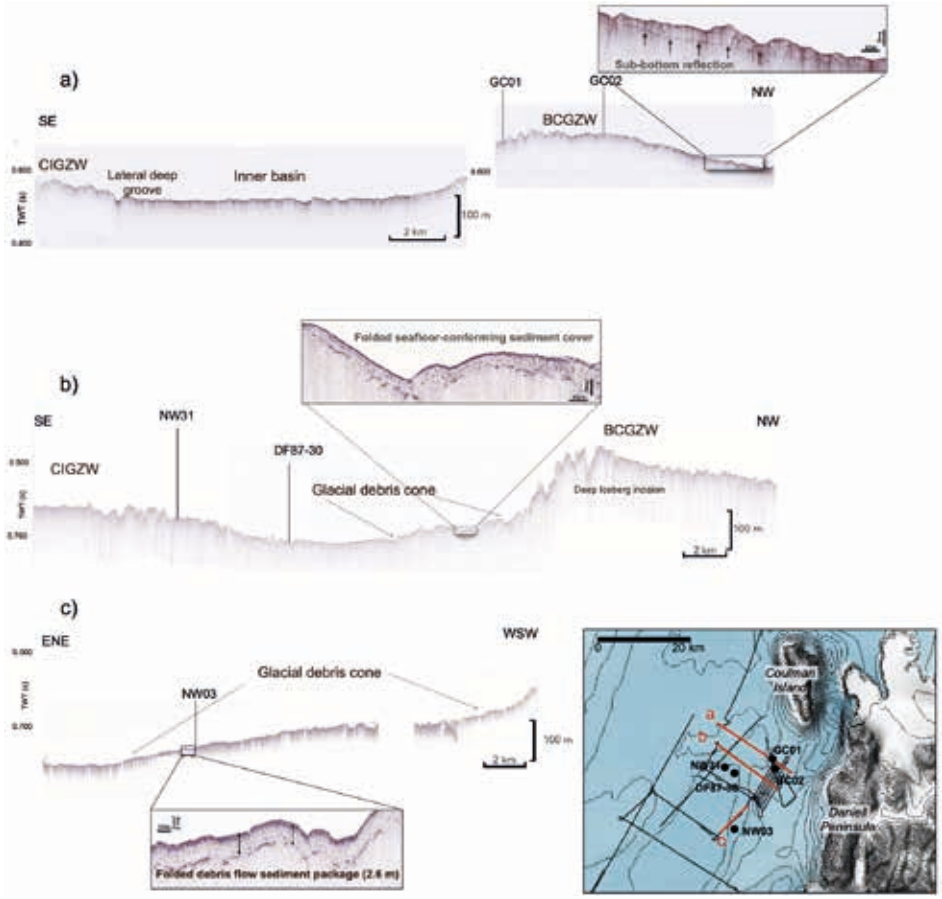


Fig. 4 - GLEVORS sub-bottom profiles through the BCGZWC area (a, b), including the frontal glacial debris flow cone (c), the CIGZW, and the bay in between. The positions of the sediment cores used are indicated along the profiles. Zoomed insets highlight the back part of the frontal wedges, where retreat moraine deposits and/or parallel or sub-parallel incisions caused by the scoring of advancing or retreating ice are visible (panel a), as well as the folded, seafloor-conforming shallow sediments of the glacial debris cone (panels b and c).

in core GC02, and a mean Mz of 4.9 ± 0.3 ϕ (coarse silt). The water content is constant (around 29%) in GC02 while it varies between 26 and 44% in GC01. The MS value is lower in GC01 than in GC02. It comprises poorly preserved biogenic limestone and the presence of pebble remains. Foraminifera (<25 specimens/g) and diatoms are rare or poorly preserved throughout the cores (Fig. 6a).

Contact between Unit 1 and the upper part of Unit 2 (at approximately 30 cm from the core top in GC02 and approximately 2 cm from the core top in GC01) is irregular and sharp.

Unit 2 is composed of dark, olive-grey to olive sandy silt with sparse IRD clasts. The Mz is 5.5 ± 0.5 ϕ (silt), the water content is 34 ± 11% in GC02 and 29% in GC01. The MS and density are more variable than in Unit 1 (average MS is 598 ± 205 SI×10^{-5} and average density is 1.43 ± 0.154 g/cc). In the smear slides, made on the pristine material after splitting, the presence of mud flakes, consisting exclusively of clay particles and without organic diatom residues, was highlighted. They are absent in the upper 10 cm of core GC02. The biogenic fraction is abundant and characterised by sponge needles, sea urchin spines, calcareous foraminifera (less than 100 specimens/g up to 14 cm, between 100 and 500 specimens/g upwards), and diatoms (with

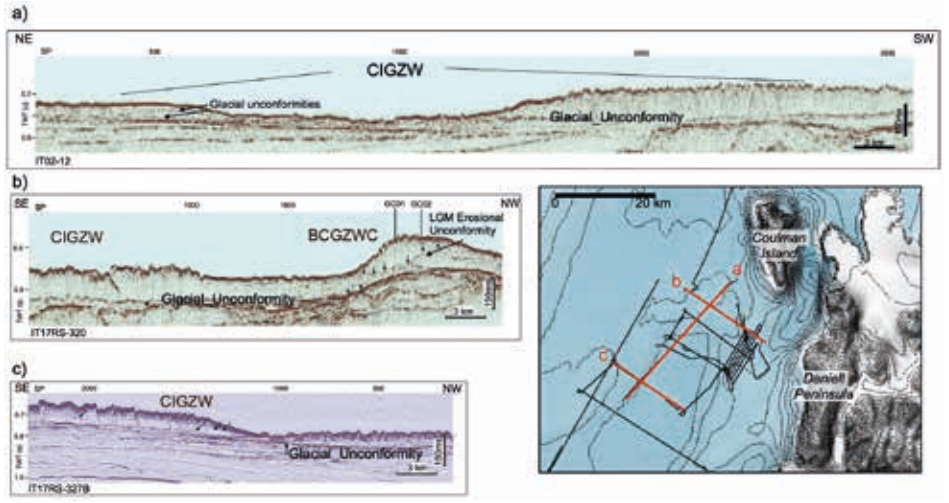


Fig. 5 - a) Single-channel seismic profile crossing the CIGZW, displaying the two sectors of the grounding zone: the southern CIGZW glacial deposit and the glacial terrace of the northern CIGZW. b) Single-channel seismic line showing the infilling sediments lying on the concave erosional unconformity of the perched valleys at the front of the BCGZWC. c) Single-channel seismic line showing the terrace of the northern CIGZW and the NW–SE prograding clinoforms.

high ADA mean values of 5.35×10^5 and a maximum value of 7.7×10^5 at 8–10 cm) (Fig. 6b). In GC01, Unit 2 has a foraminiferal density of about 230 specimens/g and an ADA value of 1.79×10^5 valves/g dry sediment. The ADA value reaches 2.15×10^5 valves/g dry sediment. Unit 2 is less than 3.5 ka BP (Table A2 in the Appendix).

4.1.3. Interpretation

The geophysical data indicate that the bank off the Borchgrevink Coast exhibits the typical features of a palaeo-GZW complex, which we designate as the BCGZWC. Given the architecture of the bank, its irregular external shape, and the various internal glacial unconformities, it is likely that the BCGZWC formed during multiple glacier oscillations up to the final stage of the LGM.

It is inferred that the NVL glaciers, specifically the Mariner and Borchgrevink glaciers, after carving the trough between the coast and Coulman Island (Anderson *et al.*, 2014), streamed in an approximately NE–SW direction (see the MS GLs in Figs. 2 and 3a), then underwent significant deflection and lateral expansion along the coast off the Daniell Peninsula, subsequently flowing seawards from the coast in different ENE–WSW, E–W, and N–S directions. This is evidenced by the MS GLs on the inner bank surface, which record the palaeo-flow directions of the Borchgrevink and Mariner glaciers during past expansions along the coastal region (Figs. 3a and 3b). The different orientations of these overlapping MS GL sets indicate changes in ice flow direction during multiple phases of glacier expansion, with the most recent direction apparently being from east to west.

The upper and frontal parts of the ice grounding wedges of the BCGZWC display seaward-prograding clinoforms that overlie the inclined erosional surface, presumably eroded by the N-S AIS advance (Fig. 5b). These clinoforms consist of sediments deposited in the resulting accommodation space (the so-called perched valleys) by the NVL coastal glaciers during their last westward advance at the LGM, as confirmed by the sampling and dating the GC02 sediment core. GC01 and GC02 cores penetrate the upper 166 cm of sediment deposited on the inclined

surface of the BCGZWC front. The physical and micropalaeontological characteristics of the lower Unit 1, interpreted as a dimicton, suggest deposition in a subglacial, ice-proximal grounding zone environment (Domack and Harris, 1998; Prothro *et al*., 2018; Smith *et al*., 2019; Robinson *et al*., 2021; Giorgetti *et al*., 2024) before 20 cal ka BP. The upper part of Unit 2 indicates a more open water environment characterised by a rich plankton and benthos ecosystem during the Late Holocene (3.5 to 0.5 cal ka BP; Table A2 in the Appendix). The significant age gap between these two units suggests the presence of a hiatus.

The frontal convex cone-like feature at the north–north-eastern edge of the BCGZWC is presumably composed of collapsed sedimentary material that forms a frontal glacial debris lobe. This lobe has partially covered the ridges and grooves on the seafloor of the western frontal seaward basin, overlying an older, rough, glacially grooved surface. The surface of this glacial debris lobe is not marked by moraines or GLs but instead by presumed gullies and, farther offshore, by meltwater channels. Both features indicate that during deglaciation, meltwater was released near the grounding zone (Figs. 3b and 3e; Table 2), as observed in the central Ross Sea (Simkins *et al*., 2017). Rather than being gullies consistent with the outer channels, an alternative interpretation of the 'paw scrape' features is that they were likely formed by the keel of a stranded iceberg that was freed in successive stages.

The NW02 and NW03 cores, located on the glacial debris flow cone (Figs. 2 and 4c), contain glaciomarine sediments dated in the middle part of core NW02 to around 19–22 cal ka BP (Table A2 in the Appendix). They record variable depositional environments, ranging from ice-proximal to ice-distal glaciomarine facies, with oscillations of the ice shelf calving line (Fig. 4c). This acoustic unit overlies a rough, highly reflective surface that is impenetrable to seismic waves and likely represents consolidated, coarser sediment previously eroded by grounding ice during earlier advances over the basin. The tephra layers found in these two cores — dated by ^{40}Ar-^{39}Ar to 72 ± 2.8 ka and 23.7 ± 5.3 ka in core NW02 (Del Carlo *et al*., 2015), and by ^{14}C between 33.8 and 15.8 kal ka BP (Di Roberto *et al*., 2024) — are part of the shallowest frontal portion of the glacial debris flow cone (landslide material and/or an older and seaward grounding zone?) that is superimposed on the basin's seafloor, particularly on the subglacial features that characterised it (Table 2). Since the 72 ka dating for NW02, one hypothesis is that some of the oldest subglacial features, and the associated grounding and erosion event of the basin's seafloor, may be older than 72 ka.

The passage of various past and present icebergs, indicating a preferred calving path, is recorded on the surface of the outer BCGZWC and the frontal debris cone. Deep furrows along the north and NE edge of the bank were created by iceberg keels scouring the seabed while drifting along a straight N-S path. Alternatively, these border furrows may record a series of stepped landslides (Fig. 3b).

4.2. Coulman Island grounding zone wedge

4.2.1. Geomorphic features and acoustic facies

The geophysical data indicate that the bank north of Coulman Island is approximately 120–125 km long and 40–45 km wide. It is divided into two sectors by a hollow nearly 75 m deep and about 13 km wide (Figs. 4, 5, 7, and 8), with the northern sector being shallower.

Multibeam data show that the seabed in both the northern and southern sectors of the bank is dominated by arcuate, randomly oriented furrows, while parallel lineations are sparse (Figs. 2 and 3c).

The geometry and acoustic facies of the sediment below the seafloor in the two sectors of

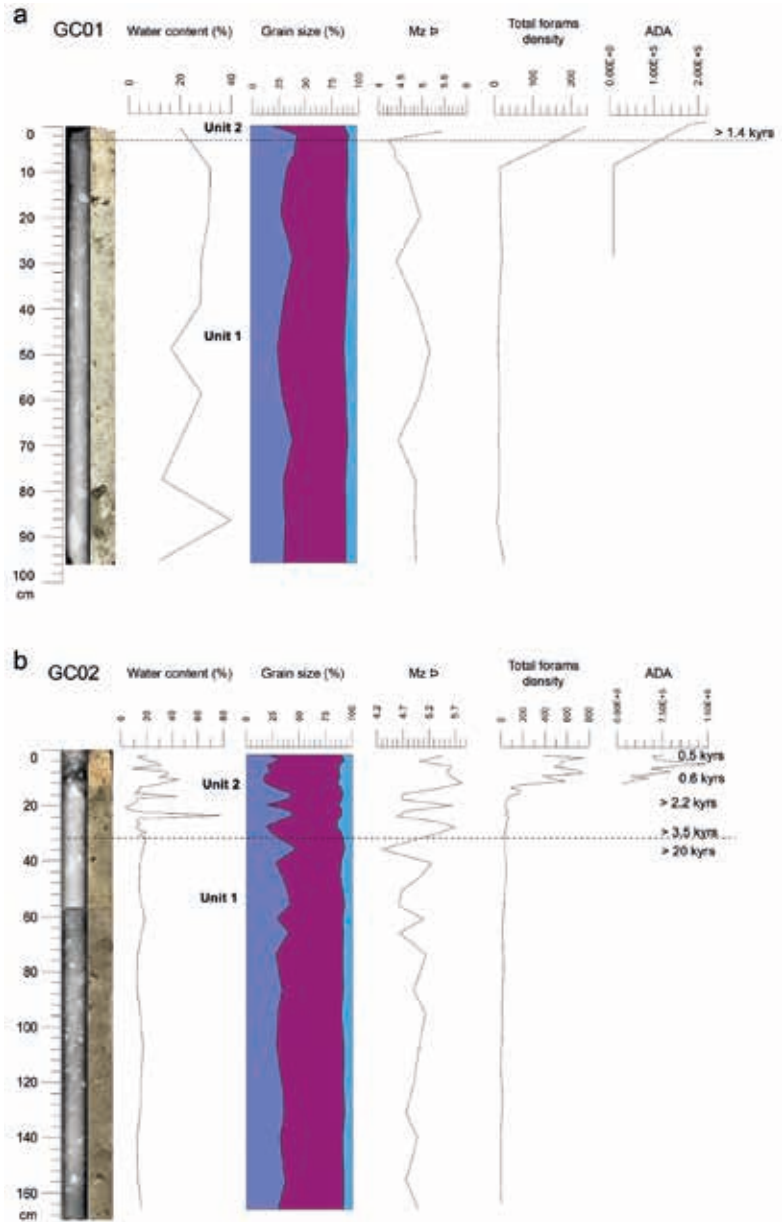


Fig. 6 - Lithostratigraphic features of the GC01 (a) and GC02 cores (b) including (left to right): X-ray image and high resolution photograph; water content (%); quantitative grain size logs; mean Mz; total forams density, expressed as n. specimens/g dry sediment; ADA.

the bank, as shown on seismic profiles (Figs. 5 and 8), are characterised by a semi-transparent acoustic lens lying on a horizontal, flat erosion surface. The upper surface of the lens is irregular and incised by sediment ridges approximately a few metres high. The seismic signature of the northern bank is locally characterised by internal reflections that are subparallel and conformable to the seafloor or inclined towards the west (Figs. 5a and 5c).

Sparkle data show sediment deposits of the southern and northern CIGZW overlying the seafloor of the southern nDB, evidently affected by ridges and grooves (in Figs. 7a and 7b, respectively). To the west of the northern CIGZW, a wedge-shaped landform is evident, with an eroded, nearly flat upper surface and internal facies characterised by NW-SE offset bank progradations (Fig. 7b).

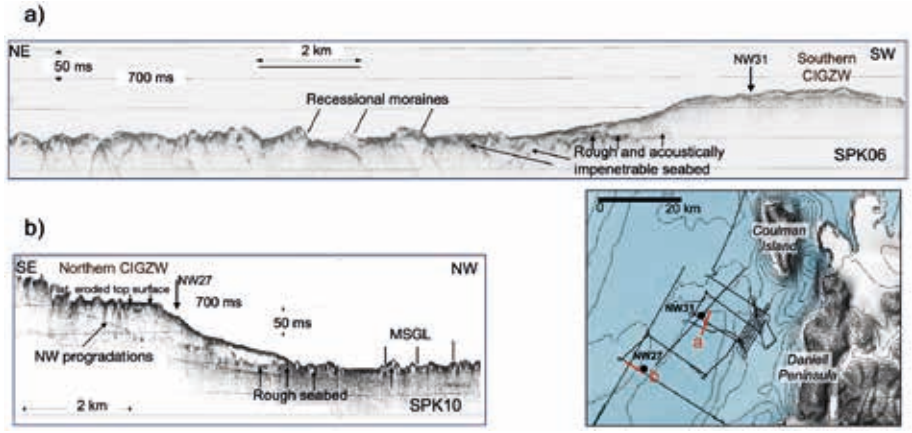


Fig. 7 - Sparker profiles (a) and (b) crossing the south-western and north-eastern margins of the CIGZW and the locations along the profiles of sediment cores NW31 and NW27. Profile (a) displays smoothed, hummocky, frontal glacial deposits with no evidence of progradation and downstream, basinal hummocky bottom morphology consisting of retreat moraines. Profile (b) shows the hummocky glacial deposits on northern CIGZW, the flat and eroded upper surface, the north-western basin progradations within the glacial deposit wedge, and, farther offshore, the basinal glacial striations visibly buried beneath the outermost foreset of the GZW.

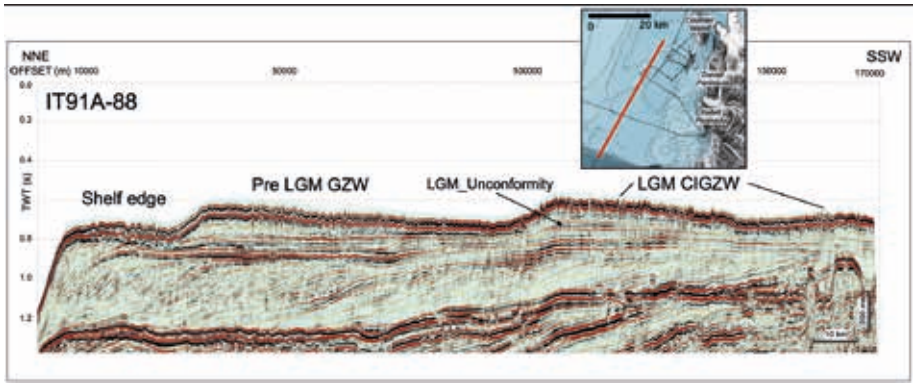


Fig. 8 - Multichannel seismic profile showing the outcropping glacial units in the nDB, with the LGM CIGZW overlying the outermost pre-LGM GZW.

4.2.2. Interpretation

We interpret the bank north of Coulman Island as a palaeo-GZW complex, confirming previous interpretations of the CIGZW (Shipp *et al*., 1999; Bart *et al*., 2011; Anderson *et al*., 2014; Halberstadt *et al*., 2016; Danielson and Bart, 2023). The Italian PNRA cores previously collected on the CIGZW, and considered in this study, are the NW31 and NW27 cores, sampled at the top of the southern sector of the CIGZW (Figs. 4b and 5a) and on the inclined flank of the northern sector of the CIGZW (Fig.5b), respectively. At the base of both cores NW31 and NW27, a subglacial diamicton with low biogenic content was recovered and dated to an age older than 30 cal ka (Table A2 in the Appendix). This diamicton is interpreted to have been deposited in an ice-proximal environment (Melis *et al*., 2002; Colizza *et al*., 2003), resembling a proglacial deposit on the foreset of the GZW and an ice-proximal basal debris meltout [facies 2 and 3 according to Prothro *et al*. (2018)]. This interpretation is consistent with the position of the cores on the top

or frontal slope of the CIGZW, although they are near the limit of the LGM palaeo-ice sheet. The sediment above the subglacial diamicton is glaciomarine and shows variable characteristics in the cores from the southern CIGZW (NW31) and from the north-eastern CIGZW (NW27).

In core NW31, the glaciomarine sediment is laminated and has high water and mud content, while in core NW27, the glaciomarine sediment contains a higher concentration of IRD and has a sandier composition. These characteristics are associated with the oscillations of the sub-ice shelf (Melis *et al*., 2002). The acoustic facies observed in the sub-bottom profile onto which the NW31 core site is projected (core site projection approximately 1 km away in Figs. 4b and 7a) has lower resolution and displays an uppermost, very shallow, hummocky, and almost transparent signature – interpreted as reworked glaciomarine sediments or reworked overriding sediments – resembling a proximal basal debris meltout [facies 3 according to Prothro *et al*. (2018)]. The intermediate sampled sediment interval in the northern NW27 core, with significant sand and low biogenic content [facies 2, after Prothro *et al*. (2018)], matches the acoustic facies observed in the sub-bottom profile nearest to the core location (core projection on the profile is nearly 100 m in Fig. 7b) and indicates a depositional environment characteristic of the foreset of an ice GZW.

The mud interval (older than 24.1 cal ka BP) in the NW31 sediment core, described as homogeneous, biogenic-rich (with an assemblage of autochthonous foraminifera), and bioturbated, has been attributed to deposition under an ice shelf far from the calving and grounding zones and related to meltwater plume deposition (Domack *et al*., 1998, 1999; Melis *et al*., 2002; Smith *et al*., 2019) [facies 4 of Prothro *et al*. (2018, 2020)].

Cores DF80-144 to DF87-32 are always positioned on the CIGZW, east and south of NW27 and NW31, respectively (Fig. 2). DF80-144 presents glaciomarine sediments aged between 35.2 and 23.3 ka recording an ice-proximal sedimentation (Licht *et al*., 1999), followed by a surficial muddy layer, Holocene in age. Core DF83-32, located in the southern position, has a stratigraphy comparable to that of NW31, being characterised by glaciomarine sediments overlaid by muddy sediments containing two layers of tephra. Radiocarbon dates from the sediments above and below the tephra layers (Table A2 in the Appendix) show that deposition conditions occurred between 21.5 and 30 ka (Licht *et al*., 1999).

The geomorphology and seismic signature of the CIGZW indicate ice streaming towards the NE. The ice likely expanded from the David Glacier, possibly converging with other ice streams from the south, and became anchored on the bank behind the Coulman High and on the Mawson Bank. At this location, a GZW formed, prograding north and west where there was enough space to accommodate sediments, possibly during a period of ice sheet stillstand before the ice retreated (Figs. 7a and 7b). The CIGZW overlies an older GZW near the continental shelf margin (Fig. 8), providing evidence that: i) the backstepping retreat of grounding ice occurred in a NE–SW/NNE–SSW direction, punctuated by temporary halts; and ii) the Mawson Bank acted as a pinning point during multiple ice sheet advances and retreats.

4.3. The basin between the Coulman Island and Borchgrevink ice grounding zones

4.3.1. Geomorphic features and acoustic facies

The basin between the CIGZW and the BCGZWC has a depth ranging from 500 m in the southernmost area to 600 m in the north. In the southern, shallower inner part of the basin, the seafloor is marked to the east by ridges and grooves with a predominant N–S direction, and to the west by deeper, more widely spaced furrows, some of which oriented NE–SW (Figs. 3c and 4a).

About 10 km to the north/NE, multibeam observations have identified an area of the basin with no obvious lineations but with V-shaped furrows whose apex points in the SSE direction and pit scours (Fig. 3c and Table 2). Moving further NE, where the basin is deeper and wider, the seafloor is characterised by more irregular NNE–SSW and NE–SW (more offshore) grooves (Fig. 3d and Table 2). The seafloor features observed in the basin off the northern CIGZW consist of sparse corrugation ridges embedded within linear, parallel lineations and generally oriented at a 45° angle to these lineations (Fig. 3e and Table 2).

4.3.2. Interpretation

The southern inner part of the basin between the BCGZWC and CIGZW displays N–S MS GL imprinted on glacial material transported by the marine ice sheet and likely by the southern NVL glaciers, which flow from the bays between Cape Washington and Coulman Island. The V-shaped furrows with the apex pointing SSE and the pit plough marks observed in the northern zone may represent footprints formed by sub-ice stranded keels as the ice stream slowed and stopped. The more external, deeper basin area, marked by irregular NNE–SSW and NE–SW (more offshore) grooves on the seabed, has been eroded to varying degrees by the passage of ice keels. In the basin, this 50 km long ice-keel *mélange* zone (Table 2) formed with glacial striations and ice furrows predominantly in a NE–SW direction (Smith *et al*., 2019), possibly due to a broken ice shelf forced to advance between the lateral ice sheet and the coastal glaciers, at least initially and for several tens of kilometres. This is interpreted as evidence of ice shelf disintegration. The seafloor features observed in the basin area off the northern CIGZW, such as corrugation ridges nested perpendicularly or obliquely within GLs (Table 2), resemble the 'washboard pattern' corrugation ridges described by Jakobsson *et al*. (2011) and interpreted as resulting from the grounding and ungrounding of ice keels in response to tidal motion. This evidence suggests that the collapse of an existing ice shelf may have occurred when the ice was still relatively thick or the sea level was relatively low, allowing the keels of the broken ice shelf to erode and corrugate the soft sediment on the seafloor. The breakup would have destabilised and accelerated the upstream ice and propelled an armada of icebergs from the broken ice shelf.

Core DF87-30, located in the basin between the CIGZW and the BCGZWC, contains glaciomarine sediments overlain by a thin interval of muddy sediments with two tephra layers. Although these layers have not been dated, their chemical composition, which is similar to that of Mount Melbourne, suggests a deposition age of 10 ± 20 ka BP (Licht *et al*., 1999).

5. Discussion

In the following discussion, we present the results comprehensively and inclusively, incorporating all combined geophysical and geological data used. We address several aspects, including some that are controversial, and place them in the context of current literature, comparing them with previous work. We also summarise potential future developments in the nDB.

We have traced the grounding line at the LGM in the southern nDB, indicating the maximum expansion of the ice sheet and NVL glaciers, as defined by the prominent CIGZW and the coastal BCGZWC that served as strategic ice pinning points. Furthermore, different deglaciation behaviours between localised NVL glaciers and the main AIS have been evidenced.

The study of sedimentary successions recording the transition from subglacial diamicton to glaciomarine sediments (Figs. 9 and 10) provides valuable evidence for constraining the position

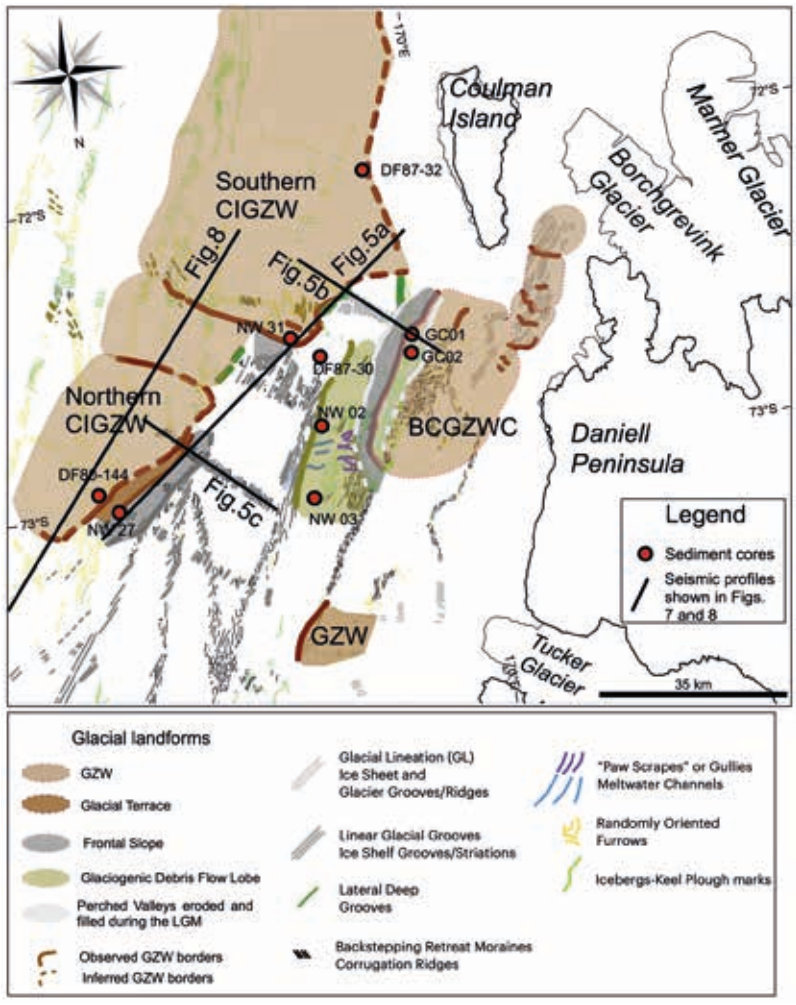


Fig. 9 - Schematic diagram of glacial landforms and small-scale features based primarily on seafloor mapping and, for the GZW margins, also on subseafloor and seismic profiles (solid brown lines where boundaries appear as frontal wedge shapes on seismic or acoustic profiles, or very thick or thin brown dots where interpolations or no data are available). The locations of all sediment cores mentioned in the paper and the seismic profiles shown in Figs. 5 and 8 are indicated. All glacial features shown are listed in the box below.

of the grounding line. However, radiocarbon ages obtained from these sediments do not always reflect the timing of the maximum ice sheet expansion during the LGM. The sediment cores located north and south of the CIGZW (NW27 and NW31) indicate that the underlying subglacial diamicton is older than 30 ka, whereas the overlying glaciomarine succession, indicating the onset of the ice sheet retreat, yields ages between 24 and 30 ka, spanning Marine Isotope Stage (MIS) 3-MIS 2 transition (Fig. 10). In contrast, the cores collected along the Borchgrevink Coast provide a minimum age for the subglacial sediment that is consistent with the presence of the ice sheet during the LGM.

The occurrence of radiocarbon ages older than expected for sediments deposited during the post-LGM retreat may have two plausible explanations. First, radiocarbon chronologies based on the fraction of acid insoluble organic matter may be biased by contamination from reworked ancient organic carbon released through glacial erosion and/or the remobilisation of unconsolidated sediments, a process that is widely documented in the literature [for a discussion, see Andrews *et al*. (1999), Mezgec *et al*. (2017), and Tesi *et al*. (2020)]. Alternatively, the maximum expansion of the ice sheet may have occurred prior to the LGM, followed by fluctuations between 30 and 20 ka that permitted the deposition of glaciomarine sediments and tephra layers (Fig. 10).

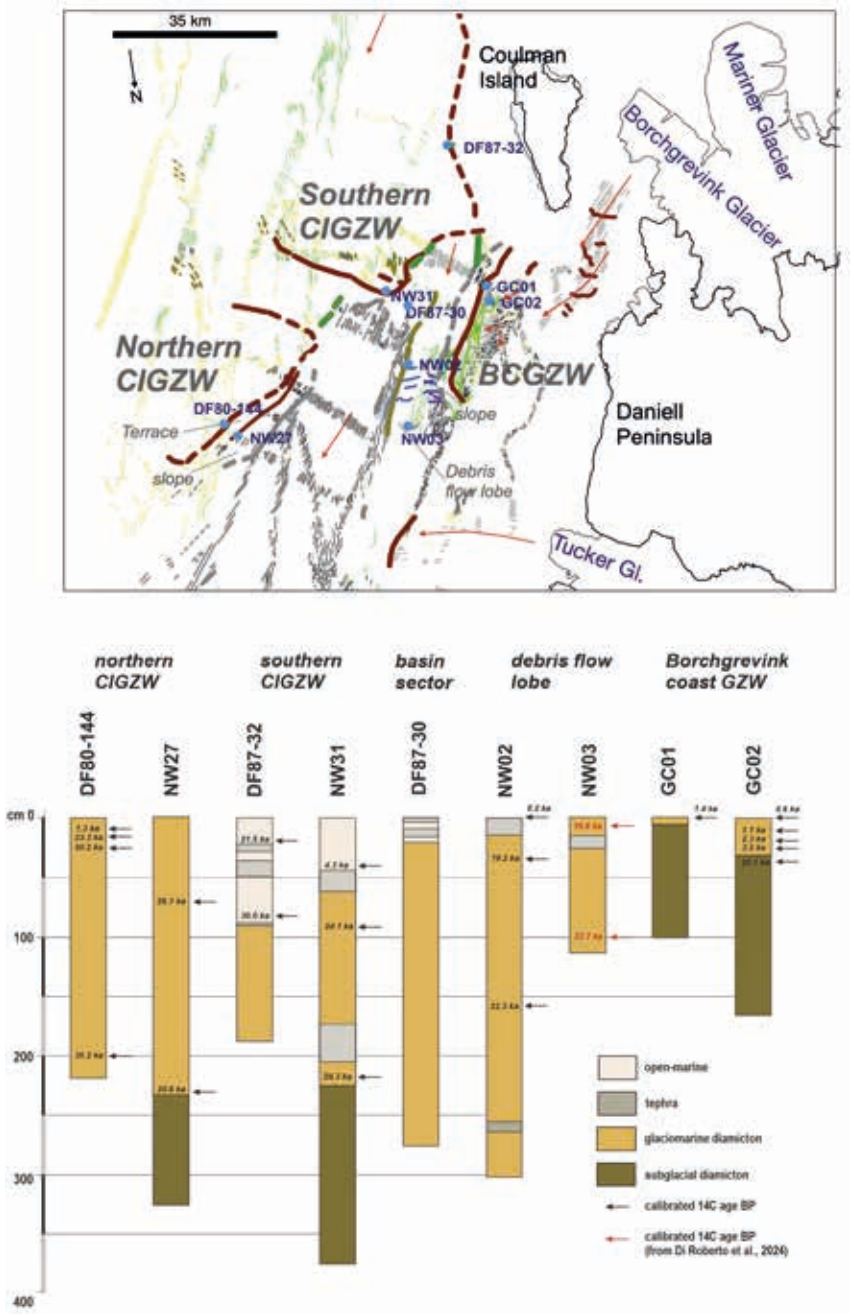


Fig. 10 - Simplified stratigraphy of the cores analysed in the text. Cores DF80-144, DF87-30, and DF87-32 are taken from Licht *et al*. (1999); cores NW02, NW03, NW27, and NW31 are taken from Melis *et al*. (2002), Colizza *et al*. (2003) and Del Carlo *et al*. (2015); cores GC01 and 02 are presented in this work. The black arrows indicate the ages that have been recalibrated (see Table A2 in the Appendix), while the red arrows indicate the dates already calibrated by Di Roberto *et al*. (2024). The radiocarbon age of cores GC01 and GC02 are presented in this work. The upper map shows the locations of the cores in relation to the interpreted main morphological features and underwater landforms, such as the CIGZW and BCGZW complex, the basin between the glacial morphological banks, the slopes in front of them, and the glacial debris flow cone in front of the BCGZWC. Glacial surficial features are indicated by different colours: subglacial and sub–ice shelf lineations in grey, iceberg plough marks in pea green, lateral grooves in dark green, inferred GLs in olive green, randomly oriented furrows in yellow, and recessional moraines and corrugation ridges in black. Palaeo-ice flows are indicated with red arrows.

The Borchgrevink–Mariner glaciers advanced along the Borchgrevink Coast, forming the composite GZW complex in several phases throughout the Late Pleistocene and Holocene. The hypothesis that the construction of the BCGZWC began at least 72 ka ago is supported by the dating of the sampled primary tephra layer (NW02), its interpretation in sub-bottom profiles in the superficial part of the debris cone in front of the BCGZWC, and, based on morphobathymetric data, by the debris cone overlying the basin's glacial features (Table 2). In contrast, the shallow sediment section at the BCGZWC front records the most recent extent of the NVL coastal glaciers during the LGM, as indicated by seismic and acoustic interpretations and new dating results from the GC02 core. These LGM shallow sediments prograde eastwards on an erosional surface that we have hypothesised was excavated by a previous N–S AIS advance (Fig. 5b). This reconstruction, which involves the hollowing and subsequent filling of the hanging valleys by the eastward-flowing Borchgrevink–Mariner coastal glaciers, indicates asynchronous oscillation of the AIS and NVL valley glaciers, as well as the persistence and late retreat of the NVL valley glaciers. The overlapping, multi-directional MSGL on the BCGZWC demonstrate that coastal glaciers advanced in distinct, diachronous steps rather than as single, uniform fronts along the coastal grounding zone during the last glacial cycle (Fig. 3b and Table 2).

The nDB was extensively eroded by grounded ice streams, as shown by widespread subglacial lineations and scouring marks on the two lateral morphological banks and within the basin. Older features are likely present within the basin, where it is hypothesised that some relict morphological features formed when the rough and hard surface beneath the GZW developed before the LGM. As hypothesised on the basis of the ^{40}Ar-^{39}Ar age constraint of 72 ka provided by the tephra layers within the mass-wasting glacial debris cone, which slipped in front of the north-eastern side of the BCGZWC and covered the glacial grooves on the basin floor (Table 2), ice grounding and basin floor excavation may have occurred during or before MIS 4 (57–71 ka). Our interpretation of seismic and acoustic data confirms that the LGM sedimentary deposits on both glacial morphological banks of the southern nDB, overlie the pre-LGM unconformity, corresponding to Unconformity 2 of Bart *et al*. (2011) that represents one of the two main AIS expansion from internal to distal continental shelf since the glacial event of Unconformity 3 (inferred 0.7 Ma; Figs. 4, 5, 7, and 8).

The southern palaeo-NVL glaciers flowing off the coast between 73°S and 75°S, along with the EAIS outlet David Glacier, reached the CIGZW in both the south and north, with varying ice flow directions. The subparallel erosional unconformities observed within the northern bank of the CIGZW, which are either even (completely flat) or uneven (wavy surfaces with ridges and grooves; Fig. 5a) — possibly resulting from grounded or ungrounded events or varying rates of ice retreat — together with the hummocky deposits in the southern CIGZW (Fig. 5b), associated with sediment reworking, are likely related to multiple ice fluctuations since at least the LGM.

In the north-eastern and eastern front areas of the BCGZWC, valley glaciers retreated to a seaward-sloping surface, possibly triggering landslides such as the one that formed the frontal debris cone after 72 ka. Clear backstepping retreat features are present on top of the BCGZWC (Fig. 3b) but are absent over the CIGZW, suggesting that the NVL glaciers experienced a different and possibly slower withdrawal, with a diachronous response to climate compared to the AIS, especially the David Glacier.

Morphobathymetric evidence, including gullies and meltwater channels on the surface of the glacial debris flow cone in front of the BCGZWC, supports the hypothesis of a subglacial meltwater system during ice withdrawal that may have prevented uniform sedimentation (Fig. 3e and Table 2).

After the LGM, the David Glacier outlet and the southern NVL glaciers that built up the CIGZW retreated rapidly once they decoupled from the basinal areas and the Mawson Bank, possibly because increased marine ice sheet instability resulted from the landward-deepening morphology of the Drygalski Basin. In contrast, as indicated by the recessional moraines on the BCGZWC surface (Fig. 3b and Table 2) and by the younger age of the diamicton sampled on the BCGZWC compared with that sampled on the CIGZW (assuming the hypothesis of a maximum advance of the ice sheet before the LGM is valid; Table A2 in the Appendix), the Borchgrevink and Mariner coastal glaciers retreated in a backstepping manner over a relatively short inland distance because their catchment basins are confined within the TAM. Morphological banks of the nDB acted as pinning points during the LGM and post-LGM ice retreat, while subglacial and ice-proximal diamicton deposits of the CIGZW and BCGZWC rimmed the banks.

In the basin area between the CIGZW and BCGZWC and their frontal sediment flanks, the ice first became ungrounded, forming a grounding line embayment with an ice shelf that persisted likely only during the initial phases of the LGM. In this area, sub-ice shelf to ice-distal glaciomarine sediments were deposited, as indicated by laminated mud containing primary tephra layers in the NW31 core (Fig. 10).

The sedimentary hiatus of approximately 14 ka at the top of the glacial-marine diamicton, observed in cores DF80-144 (Licht *et al*., 1996, 1999) and in cores NW31, NW03, and NW02 (Melis *et al*., 2002; Colizza *et al*., 2003), has been attributed to non-deposition beneath an ice shelf, scouring by an ice shelf or iceberg keel, or deglacial processes such as basal melting. This hiatus is also present in the newly studied core GC02 (transition from Unit 1 to Unit 2 in Fig. 6b). Based on this dating gap, a post-LGM floating ice shelf, anchored to the morphological banks, could have existed since 20 ka, when the grounding line was retreating and possibly connected to subglacial meltwater.

Additional morpho-bathymetric data from the basin provide further evidence for a post-LGM ice shelf, showing a *mélange* ice shelf keel zone with scour extending at least 50 km from the southern inner point of the grounding line embayment (Figs. 3d, 3e, and 9), along with evidence of the 'washboard' pattern (Fig. 3e and Table 2).

The abundance of foraminifera in LGM and post-LGM from the northern sector of the nDB, (Taviani *et al*., 1993, Frank *et al*., 2014) may suggest incursions of the warm circumpolar deep water into the basin through the Adare Trough and Wilson Canyon, which connect the western outer shelf to the open ocean (see Fig. 1). These direct connections and the resulting warm water intrusions could explain why the ice sheet did not ground on the sea floor in the basin between the CIGZW and the BCGZWC, as well as the triggering and acceleration of the retreat of a floating ice shelf first and of the grounding ice later during deglaciation, as observed in the JOIDES Basin (Melis *et al*. 2021; Torricella *et al*., 2021; Pambianco *et al*., 2025). Contrary to expectations, the coastal Borchgrevink and Mariner glaciers did not respond more quickly to post-LGM oceanic warming than the thicker ice stream grounded over the JOIDES Basin.

The proposed timing for the MIS 4 ice expansion event (~70 ka), hence the condition of a nDB free of grounded ice or with a permanent ice shelf for nearly 100 ka up to the LGM, aligns with evidence of open sea coastal conditions during 43–27 ka (Emslie *et al*., 2007). It is also consistent with data indicating that the McMurdo area was free of an ice shelf between MIS 5e (120 ± 6 ka) and the LGM (Stuiver *et al*., 1981; Denton and Hughes, 2000; McKay *et al*., 2012). Furthermore, this interpretation accords with Bart *et al*. (2011), who identified the Pleistocene uppermost glacial Unit 1/LGM Units 2-3 in the nDB. Their dating is based on the similarity of diatom assemblages in piston cores from the basin and a coeval McMurdo sediment section, as well as evidence for the main AIS expansion from the internal to the

distal continental shelf since the glacial event of Unconformity 3, with an inferred age of 0.7 Ma (Bart *et al*., 2011).

While regional frameworks (Anderson *et al*., 2014; Halberstadt *et al*., 2016; Prothro *et al*., 2020) mapped a generalised grounding line corridor near Coulman Island, our data refine these boundaries, and the GC02 sediment core provides precise temporal constraints confirming the late, persistent advance of the coastal NVL glaciers during the LGM.

Sedimentological attributes from cores NW31 and NW27 confirm the proximal-to-distal grounding-line depositional facies (facies 2, 3, 4, and 5) evidenced by Prothro *et al*. (2018, 2020), validating local alternations between sub-ice shelf and open-marine environments during and after the LGM.

The deglaciation of valley glaciers along the north-eastern BCGZWC and of the AIS along the southern and northern CIGZW was likely characterised by local, heterogeneous processes, as the modern, complex spatial retreat patterns documented for the Thwaites Glacier in West Antarctica (Milillo *et al*., 2019).

The literature has documented a difference between the SVL and NVL glaciers, particularly in their response to sea level rise related to deglaciation: the response is linear for the glaciers of NVL and nonlinear, i.e. irreversible and causing marine ice sheet instability (MISI), for those of SVL (Goehring *et al*., 2019).

Our analysis considered USAP DF87-30 and DF87-32 (Licht *et al*., 1999) and Italian NW31, NW02, and NW03 (Colizza *et al*., 2003) core interpretations, which used unweathered volcanic glass to argue against a large LGM ice shelf. By integrating the ^{40}Ar-^{39}Ar dating of Del Carlo *et al*. (2015) and coastal penguin nesting constraints [35–18 ka: Baroni and Orombelli (1994)], we propose a dynamic seasonal sea-ice and meltwater-pond mechanism instead of a permanent ice-shelf model.

For potential future research developments in this area, the following points should be considered:

i) expand the investigation area from the southernmost part of the nDB northwards to reconstruct the glacial history of valley glaciers along the entire Borchgrevink Coast, up to the shelf edge, consistently integrating geophysical data and sediment cores already acquired and those that may be acquired in the future;
ii) conduct higher-resolution sub-bottom seismic profiling, particularly across the CIGZW, to resolve low-resolution, quasi-transparent acoustic signatures and to map precise sediment reworking boundaries and subsurface erosional unconformities;
iii) carry out a coring survey targeting deeper layers to date the subsurface erosional unconformities;
iv) provide precise constraints for numerical ice sheet modelling.

6. Conclusions

This work is the first investigation and mapping of an ice grounding deposit along the Borchgrevink Coast off NVL, that we name the BCGZWC. Together with the CIGZW, it represents one of the two most important complex ice-grounding zones in the north-westernmost Ross Sea.

A combined geophysical and geological analysis of glaciomarine sediments on the mid-outer shelf of the north-western Ross Sea reveals erosion and ice-grounding events associated with asynchronous advances of the AIS and TAM valley glaciers from the neighbouring western Borchgrevink Coast during the Late Pleistocene–Holocene.

The results are as follows:

i) the NVL Borchgrevink glaciers formed an ice grounding zone complex (BCGZWC) along the coastal Borchgrevink area likely in the Late Pleistocene and during their last glacial advance, probably with ENE–WSW, E–W, and N–S ice flow directions. The outer, uppermost part of the BCGZWC complex consists of prograding sediments that filled perched valleys at the edge of the grounding zone. These valleys were excavated by a N–S advance of the AIS and subsequently filled with sediments from the NVL valley glaciers that advanced in an E–W direction during the LGM;
ii) analysis and dating of the two GLEVORS sediment cores confirmed their deposition in a proximal grounding zone environment during the last glacial period, and the development of a rich plankton and benthos ecosystem during the Late Holocene (less than 4,000 years ago);
iii) based on available data, it is hypothesised that the basin between the CIGZW and the BCGZWC likely preserves a record of past environmental conditions since MIS 4, approximately 71 ka ago. Additional shallow drilling of the upper metres of thick sediments in this area would enable to clarify the processes responsible for ice sheet and ice shelf retreat, as well as the interactions among ocean, ice, and bedrock, possibly during MIS 2. Such records are extremely rare in Antarctica, especially on the continental shelf and in coastal areas;
iv) the submarine grounding line indentation zone between the CIGZW and the BCGZWC shows evidence of an ungrounded ice shelf (ice keel *mélange* zone) and possibly its collapse, which may be related to the onset of MIS 4 (71–57 ka), and/or the more recent end of the LGM at the end of MIS 2 (29–14 ka). For the last glaciation period, a dynamic seasonal sea-ice/meltwater-pond mechanism is hypothesised rather than a permanent ice shelf. During the LGM, an absent (collapsed?) or greatly reduced ice shelf would have prevented the ice sheet from advancing further into the basin, while after the LGM, the ice shelf likely formed and persisted throughout deglaciation;
v) the AIS and Borchgrevink–Mariner valley glaciers showed different dynamics and flow directions, expanding asynchronously. The grounding line edge, where the AIS and NVL glaciers decoupled from the seafloor, underwent local deglaciation processes such as gravitational sliding and meltwater activity at the north-eastern edge of the BCGZWC in front of the coastal glaciers or at the southern CIGZW. The NVL glaciers would have experienced a delayed, stable retreat compared to the rapid, MISI-driven retreat of the AIS.

Acknowledgments. This study was funded by the PNRA in the framework of the GLEVORS and VILD projects. The authors acknowledge S&P Global for the academic licence of Kingdom™ Geoscience Software for seismic interpretation. The data used were collected during several PNRA cruises. The multichannel seismic profile (IT91A-88) is available through the Antarctic Seismic Data Library System for Cooperative Research (Istituto Nazionale di Oceanografia e di Geofiscia Sperimentale – OGS, n.d.). The multibeam data used in this paper are available in Dorschel *et al.* (2022) or the GMRT Data Synthesis hosted at the Lamont-Doherty Earth Observatory of Columbia University. The PNRA cores are stored at the Sorting Center of the Italian National Antarctic Museum Section of Trieste (Museo Nazionale dell'Antartide, n.d.).

REFERENCES

Alley R.B., Anandakrishnan S., Dupont T.K., Parizek B.R. and Pollard D.; 2007: *Effect of sedimentation on ice-sheet grounding-line stability.* Science, 315(5819), 1838–1841, doi: 10.1126/science.1138396.

Anderson J.B., Kennedy D.S., Smith M.J. and Domack E.W.; 1991: *Sedimentary facies associated with Antarctica's floating ice masses*. In: Anderson J.B. and Ashley G.M. (eds), Glacial marine sedimentation; Paleoclimatic significance, Geological Society of America Special Paper, 261, pp. 1-25.

Anderson J.B., Shipp S.S., Lowe A.L., Wellner J.S. and Mosola A.B.; 2002: *The Antarctic ice sheet during the Last Glacial Maximum: its size and configuration.* Quaternary Science Reviews, 21(1-3), 49–70, doi:10.1016/S0277-3791(01)00082-5.

Anderson J.B., Conway H., Bart P.J., Witus A.E., Greenwood S.L., McKay R.M., Hall B.L., Ackert R.P., Licht K., Jakobsson M. and Stone J.O.; 2014: *Ross Sea paleo ice sheet drainage and deglacial history during and since the LGM*. Quat. Sci. Rev., 100, 31-54, doi: 10.1016/j.quascirev.2013.08.020.

Andrews J.T., Domack E.W., Cunningham W.L., Leventer A., Licht K.J., Jull A.J.T., DeMaster D.J., Jennings A.E.; 1999: *Problems and possible solutions concerning radiocarbon dating of surface marine sediments, Ross Sea, Antarctica.* Quat. Res., 52, 206-216, doi: 10.1006/qres.1999.2047.

Baradello L.; 2014: *An improved processing sequence for uncorrelated Chirp sonar data*. Mar. Geophys. Res., 35, 337-344, doi: 10.1007/s11001-014-9220-1.

Barde M.F.; 1981: *Les diatomées des sédiments actuels et du Quaternaire supérieur de l'Atlantique Nord-Oriental. Intérêt hydrologique et climatique*. Bull. Inst. Géol. Bassin Aquitaine, 29, 85-111.

Baroni C. and Orombelli G.; 1994: *Abandoned penguin rookeries as Holocene paleoclimatic indicators in Antarctica*. Geology, 22, 23-26, doi: 10.1130/0091-7613(1994)022<0023:APRAHP>2.3.CO;2.

Bart P.J. and Anderson J.B.; 2000: *Relative temporal stability of the Antarctic ice sheets during the late Neogene based on the minimum frequency of outer shelf grounding events.* Earth and Planetary Science Letters, 182(3-4), 259–272, doi: 10.1016 /S0012-821X(00)00245-8.

Bart P.J., Anderson J.B., Trincardi F. and Shipp S.S.; 2000: *Seismic data from the Northern basin, Ross Sea, record extreme expansions of the East Antarctic Ice Sheet during the late Neogene*. Mar. Geol., 166, 31-50, doi: 10.1016/S0025-3227(00)00006-2.

Bart P.J., Sjunneskog C. and Chow J.M.; 2011: *Piston-core based biostratigraphic constraints on Pleistocene oscillations of the West Antarctic Ice Sheet in western Ross Sea between North Basin and AND-1B drill site*. Mar. Geol., 289, 86-99, doi: 10.1016/j.margeo.2011.09.005.

Bentley M.J., Ó Cofaigh C., Anderson J.B., Conway H., Davies B., Graham A.G.C., Hillenbrand C.-D., Hodgson D.A., Jamieson S.S.R., Larter R.D., Mackintosh A., Smith J.A., Verleyen E., Ackert R.P., Bart P.J., Berg S., Brunstein D., Canals M., Colhoun E.A., Crosta X., Dickens W.A., Domack E., Dowdeswell J.A., Dunbar R., Ehrmann W., Evans J., Favier V., Fink D., Fogwill C.J., Glasser N.F., Gohl K., Golledge N.R., Goodwin I., Gore D.B., Greenwood S.L., Hall B.L., Hall K., Hedding D.W., Hein A.S., Hocking E.P., Jakobsson M., Johnson J.S., Jomelli V., Jones R.S., Klages J.P., Kristoffersen Y., Kuhn G., Leventer A., Licht K., Lilly K., Lindow J., Livingstone S.J., Massé G., McGlone M.S., McKay R.M., Melles M., Miura H., Mulvaney R., Nel W., Nitsche F.O., O'Brien P.E., Post A.L., Roberts S.J., Saunders K.M., Selkirk P.M., Simms A.R., Spiegel C., Stolldorf T.D., Sugden D.E., van der Putten N., van Ommen T., Verfaillie D., Vyverman W., Wagner B., White D.A., Witus A.E. and Zwartz D.; 2014: *A community-based geological reconstruction of Antarctic Ice Sheet deglaciation since the Last Glacial Maximum*. Quat. Sci. Rev., 100, 1-9, doi: 10.1016/j.quascirev.2014.06.025.

Bodén P.; 1991: *Reproducibility in the random settling method for quantitative diatom analysis*. Micropaleontology, 37, 313-319.

Brancolini G., Busetti M., Coren F., De Cillia C., Marchetti M., De Santis L., Zanolla C., Cooper A.K., Cochrane G.R., Zayatz I., Belyaev V., Knyazev M., Vinnikovskaya O., Davey F.J. and Hinz K.; 1995: *ANTOSTRAT Project, seismic stratigraphic atlas of the Ross Sea, Antarctica.* In: Cooper A.K., Barker P.F. and Brancolini G. (eds), Geology and Seismic Stratigraphy of the Antarctic Margin, Antarctic Research Series, 68. AGU Washington D.C., 22 plates.

Carbotte S., Ryan W., O'Hara S., Arko R., Goodwillie A., Melkonian A., Weissel R. and Ferrini V.; 2007: *Antarctic multibeam bathymetry and geophysical data synthesis: an on-line digital data resource for marine geoscience research in the Southern Ocean.* Open-File Report 2007-1047-SRP-002, U.S. Geological Survey, 4 pp., doi:10.3133/ofr20071047SRP002.

Civile D., Crispini L., Ruppel A., Ferrante G.M., Morelli D., Accettella D., Accaino F., Locatelli M., Volpi V., Busetti M., Armadillo E. and Läufer A.; 2025: *Discovery of Cenozoic magmatic ridges and tectonics off northern Victoria Land provides new insights into the geodynamics of the Antarctic margin*. Sci. Rep., 15, 20303, doi: 10.1038/s41598-025-06739-7.

Colizza E., Finocchiaro F., Marinoni L., Menegazzo Vitturi L. and Brambati A.; 2003: *Tephra evidence in marine sediments from the shelf of the Western Ross Sea*. Terra Antarct. Rep., 8, 121-126.

Cooper A.K., Davey F.J. and Behrendt J.C.; 1987: *Seismic stratigraphy and structure of the Victoria Land Basin, western Ross Sea, Antarctica.* In: Cooper A.K. and Davey F.J. (eds), The Antarctic continental margin: geology and geophysics of the Western Ross Sea, CPCEMR, Earth Sci Ser 5B, pp. 27–76.

Corradi N., Fierro G., Finocchiaro F., Ivaldi R. and Pittà A.; 2003a: *Late Quaternary sedimentation in the Northern Western Basin, Ross Sea, Antarctica: seismostratigraphic features and sedimentary properties of calibrated cores*. In: Fütterer D.K. (ed.), Antarctic Contributions to Global Earth Science, Proceedings of the 9th International Symposium on Antarctic Earth Sciences (ISAES), 8-12 September 2003, Potsdam (Germany), Terra Nostra, pp. 55-56.

Corradi N., Fierro G., Giordano F., Ivaldi R., Nicotra G. and Pittà A.; 2003b: *Northern Western Basin (Ross Sea, Antarctica): seismostratigraphic characteristics and physical properties of the recent sedimentary deposits. Preliminary results*. Terra Antarct. Rep., 9, 77-82.

Cunningham W.L., Leventer A., Andrews J.T., Jennings A.E. and Licht K.J.; 1999: *Late Pleistocene-Holocene marine conditions in the Ross Sea, Antarctica: evidence from the diatom record*. Holocene, 9, 129-139, doi: 10.1191/095968399675562.

Danielson M.A. and Bart P.J.; 2023: *The staggered retreat of grounded ice in Ross Sea, Antarctica since the LGM*. EGUsphere, doi: 10.5194/egusphere-2023-1397.

Danielson M.A. and Bart P.J.; 2024: *The staggered retreat of grounded ice in the Ross Sea, Antarctica, since the Last Glacial Maximum (LGM)*. The Cryosphere, 18(3), 1125–1138, doi: 10.5194/tc-18-1125-2024.

Denton G.H. and Hughes T.; 2000: *Reconstruction of the Ross ice drainage system, Antarctica, at the last glacial maximum.* Geografiska Annaler, Series A, Physical Geography, 82(2-3), 143–166, doi:10.1111/j.1468-0459.2000.00118.x.

Di Roberto A., Del Carlo P., Bertagnini A., Colizza E., Pompilio M., Giglio F. and Florindo F.; 2024: *Silica spherules in Late Pleistocene–Holocene glaciomarine sediments from the Ross Sea, Antarctica: insights into the formation and significance.* Annals of Geophysics, 67, CO322, doi:10.4401/ag-9102.

Del Carlo P., Di Roberto A., Di Vincenzo G., Bertagnini A., Landi P., Pompilio M., Colizza E. and Giordano G.; 2015: *Late Pleistocene-Holocene volcanic activity in northern Victoria Land recorded in Ross Sea (Antarctica) marine sediments*. Bull. Volcanol., 77, 36, doi: 10.1007/s00445-015-0924-0.

Domack E.W. and Harris P.T.; 1998: *A new depositional model for ice shelves, based upon sediment cores from the Ross Sea and the Mac. Robertson Shelf, Antarctica*. Ann. Glaciol., 27, 281-284, doi: 10.3189/1998AoG27-1-281-284.

Domack E., O'Brien P., Harris P., Taylor F., Quilty P., De Santis L. and Raker B.; 1998: *Late Quaternary sediment facies in Prydz Bay, East Antarctica and their relationship to glacial advance onto the continental shelf.* Antarctic Science, 10(3), 236–246, doi: 10.1017/S095410209800030X.

Domack E.W., Jacobson E.A., Shipp S. and Anderson J.B.; 1999: *Late Pleistocene-Holocene retreat of the West Antarctic Ice-Sheet system in the Ross Sea: Part 2 - Sedimentologic and stratigraphic signature*. Geol. Soc. Am. Bull., 111, 1517-1536, doi: 10.1130/0016-7606(1999)111<1517:LPHROT>2.3.CO;2.

Dorschel B., Hehemann L., Viquerat S., Warnke F., Dreutter S., Schulze Tenberge Y., Accettella D., An L., Barrios F., Bazhenova E., Black J., Bohovo F., Davey C., De Santis L., Escutia Dotti C., Fremand A.C., Fretwell P.T., Gales J.A., Gao J., Gasperini L., Greenbaum J.S., Henderson Jencks J., Hogan K., Hong J.K., Jakobsson M., Jensen L., Kool J., Larin S., Larter R.D., Leitchenkov G., Loubrieu B., Mackay K., Mayer L., Millan R., Morlighem M., Navidad F., Nitsche F.O., Nogi Y., Pertuisot C., Post A.L., Pritchard H.D., Purser A., Rebesco M., Rignot E., Roberts J.L., Rovere M., Ryzhov I., Sauli C., Schmitt T., Silvano A., Smith J., Snaith H., Tate A.J., Tinto K., Vandenbossche P., Weatherall P., Wintersteller P., Yang C., Zhang T. and Arndt J.E.; 2022: *The International Bathymetric Chart of the Southern Ocean Version 2*. Sci. Data, 9, 275, doi: 10.1038/s41597-022-01366-7.

Emslie S.D., Coats L. and Licht K.; 2007: *A 45,000-year record of Adélie penguins and climate change in the Ross Sea, Antarctica.* Geology, 35(1), 61–64, doi:10.1130/G23011A.1.

Folk R.L. and Ward W.C.; 1957: *Brazos River bar (Texas); a study in the significance of grain size parameters.* Journal of Sedimentary Research, 27(1), 3–26, doi:10.1306/74D70646-2B21-11D7-8648000102C1865D.

Frank T.D., James N.P., Bone Y., Malcolm I. and Brenizer L.; 2014: *Late Quaternary carbonate deposition at the bottom of the world*. Sedim. Geol., 305, 1-16, doi: 10.1016/j.sedgeo.2014.02.008.

Gao Y., Salvatore M.C., Xu Q., Yang L., Sun L., Xie Z. and Baroni C.; 2022: *The occupation history of the longest-dwelling Adélie penguin colony reflects Holocene climatic and environmental changes in the Ross Sea, Antarctica*. Quat. Sci. Rev., 284, 107494, doi: 10.1016/j.quascirev.2022.107494.

Giorgetti G., Baroni C., Salvatore M.C., Gasperini L. and Polonia A.; 2024: *Post-LGM glaciomarine processes revealed by inner shelf sedimentary facies analysis (Terra Nova Bay, Western Ross Sea, Antarctica)*. Quat. Int., 697, 64-77, doi: 10.1016/j.quaint.2024.06.012.

Goehring B.M., Balco G., Todd C., Moening-Swanson I. and Nichols K.; 2019: *Late-glacial grounding line retreat in the northern Ross Sea, Antarctica*. Geology, 47, 291-294, doi: 10.1130/G45413.1.

Granot R., Cande S.C., Stock J.M., Davey F.J. and Clayton R.W.; 2010: *Postspreading rifting in the Adare Basin, Antarctica: regional tectonic consequences*. Geochem. Geophys. Geosyst., 11, Q08005, doi: 10.1029/2010GC003105.

Greenwood S.L., Simkins L.M., Halberstadt A.R.W., Prothro L.O. and Anderson J.B.; 2018: *Holocene reconfiguration and readvance of the East Antarctic Ice Sheet*. Nat. Commun., 9, 3176, doi: 10.1038/s41467-018-05625-3.

Ha S., Lee J., Bak Y., Yoo K. and Khim B.; 2023: *Paleoenvironmental reconstruction of glaciomarine sediments in the Drygalski Basin of the western Ross Sea since the Last Glacial Maximum*. Sediment. Geol., 456, 106495, doi: 10.1016/j.sedgeo.2023.106495.

Halberstadt A.R.W., Simkins L.M., Greenwood S.L. and Anderson J.B.; 2016: *Paleo-ice sheet behaviour: retreat scenarios and changing controls in the Ross Sea, Antarctica*. Cryosphere, 10, 1003-1020, doi: 10.5194/tc-10-1003-2016.

Hall B.L., Henderson G.M., Baroni C. and Kellogg T.B.; 2010: *Constant Holocene Southern-Ocean 14C reservoir ages and ice-shelf flow rates*. Earth Planet. Sci. Lett., 296, 115-123, doi: 10.1016/j.epsl.2010.04.054.

Heaton T.J., Köhler P., Butzin M., Bard E., Reimer R.W., Austin W.E.N., Bronk Ramsey C., Grootes P.M., Hughen K.A., Kromer B., Reimer P.J., Adkins J., Burke A., Cook M.S., Olsen J. and Skinner L.C.; 2020: *Marine20: the marine radiocarbon age calibration curve (0-55,000 cal BP)*. Radiocarbon, 62, 779-820, doi: 10.1017/RDC.2020.68.

Heaton T.J., Butzin M., Bard E., Bronk Ramsey C., Hughen K.A., Köhler P. and Reimer P.J.; 2023: *Marine radiocarbon calibration in polar regions: a simple approximate approach using Marine20*. Radiocarbon, 65, 848-875, doi: 10.1017/RDC.2023.42.

Istituto Nazionale di Oceanografia e di Geofisica Sperimentale – OGS; n.d.: *Antarctic Seismic Data Library System.* https://sdls.ogs.trieste.it/.

Jakobsson M., Anderson J.B., Nitsche F.O., Dowdeswell J.A., Gyllencreutz R., Kirchner N., O'Regan M.A., Alley R.B., Anandakrishnan S., Mohammad R., Eriksson B., Fernandez R., Kirshner A., Minzoni R., Stolldorf T. and Majewski W.; 2011: *Geological record of ice shelf breakup and grounding line retreat, Pine Island Bay, West Antarctica*. Geology, 39, 691-694, doi: 10.1130/G32153.1.

Lee J.I., McKay R.M., Golledge N.R., Yoon H.I., Yoo K.C., Kim H.J. and Hong J.K.; 2017: *Widespread persistence of expanded East Antarctic glaciers in the southwest Ross Sea during the last deglaciation*. Geology, 45, 403-406, doi: 10.1130/G38715.1.

Licht K.J., Jennings A.E., Andrews J.T. and Williams K.M.; 1996: *Chronology of late Wisconsin ice retreat from the western Ross Sea, Antarctica*. Geology, 24, 223-226, doi: 10.1130/0091-7613(1996)024<0223:COLWIR>2.3.CO;2.

Licht K.J., Dunbar N.W., Andrews J.T. and Jennings A.E.; 1999: *Distinguishing subglacial till and glacial marine diamictons in the western Ross Sea, Antarctica: implications for a last glacial maximum grounding line*. Geol. Soc. Am. Bull., 111, 91-103, doi: 10.1130/0016-7606(1999)111<0091:DSTAGM>2.3.CO;2.

Majewski W., Prothro L.O., Simkins L.M., Demianiuk E.J. and Anderson J.B.; 2020: *Foraminiferal patterns in deglacial sediment in the Western Ross Sea, Antarctica: life near grounding lines*. Paleoceanogr. Paleoclimatol., 35, e2019PA003716, doi: 10.1029/2019PA003716.

Matsuoka K., Hindmarsh R.C.A., Moholdt G., Bentley M.J., Pritchard H.D., Brown J. and Conway H.; 2015: *Antarctic ice rises and rumples: their properties and significance.* Earth-Science Reviews, 150, 724–745, doi:10.1016/j.earscirev.2015.09.004.

McKay R.M., Dunbar G.B., Naish T.R., Barrett P.J., Carter L. and Harper M.; 2008: *Retreat history of the Ross ice sheet (shelf) since the last glacial maximum from deep-basin sediment cores around Ross Island*. Palaeogeogr. Palaeoclimatol. Palaeoecol., 260, 245-261, doi: 10.1016/j.palaeo.2007.08.015.

McKay R.M., Naish T., Carter L., Riesselman C., Dunbar R., Sjunneskog C., Winter D., Sangiorgi F., Warren C., Pagani M., Schouten S., Willmott V., Levy R., DeConto R. and Powell R.D.; 2012: *Antarctic and Southern Ocean influences on Late Pliocene global cooling*. Proc. Natl. Acad. Sci. U.S.A., 109, 6423-6428, doi: 10.1073/pnas.1112248109.

McKay R., Golledge N., Maas S., Naish T., Dunbar G. and Kuhn G.; 2016: *Antarctic marine ice-sheet retreat in the Ross Sea during the early Holocene*. Geology, 44, 7-10, doi: 10.1130/G37315.1.

Melis R. and Salvi G.; 2009: *Late Quaternary foraminiferal assemblages from western Ross Sea (Antarctica) in relation to the main glacial and marine lithofacies*. Mar. Micropaleontol., 70, 39-53, doi: 10.1016/j.marmicro.2008.10.003.

Melis R., Colizza E., Pizzolato F. and Rosso A.; 2002: *Late Quaternary glacial marine sequences in Ross Sea (Antarctica): paleoenvironmental inferences throughout calcareous taxa*. In: Monegatti P., Cecca F. and Raffi S. (eds), Intern. Conf. Paleobiogeography & Paleoecology 2001, Piacenza and Castell'Arquato 2001, Geobios, 35 (Suppl. 1), pp. 207-218, doi: 10.1016/S0016-6995(02)00060-8.

Melis R., Capotondi L., Torricella F., Ferretti P., Geniram A., Hong J.K., Kuhn G., Khim B.-K., Kim S., Malinverno E., Yoo K.C. and Colizza E.; 2021: *Last Glacial Maximum to Holocene paleoceanography of the northwestern Ross Sea inferred from sediment core geochemistry and micropaleontology at Hallett Ridge*. J. Micropalaeontol., 40, 15-35, doi: 10.5194/jm-40-15-2021.

Mezgec K., Stenni B., Crosta X., Masson-Delmotte V., Baroni C., Braida M., Ciardini V., Colizza E., Melis R., Salvatore M.C., Severi M., Scarchilli C., Traversi R., Udisti R. and Frezzotti M.; 2017: *Holocene sea ice variability driven by wind and polynya efficiency in the Ross Sea*. Nat. Commun., 8, 1334, doi: 10.1038/s41467-017-01455-x.

Milillo P., Rignot E., Rizzoli P., Scheuchl B., Mouginot J., Bueso-Bello J.L. and Prats-Iraola P.; 2019: *Heterogeneous retreat and ice melt of Thwaites Glacier, West Antarctica.* Science Advances, 5(1), eaau3433, doi:10.1126/sciadv.aau3433.

Museo Nazionale dell'Antartide; n.d.: *Sedimenti marini.* https://mna.it/sedimenti-marini/.

Naish T.R., Powell R.D., Barrett P.J., Levy R.H., Henrys S., Wilson G.S., Krissek L.A., Niessen F., Pompilio M., Ross J., Scherer R., Talarico F., Pyne A. and the ANDRILL-MIS Science team.; 2009: *Obliquity-paced Pliocene West Antarctic ice sheet oscillations*. Nature, 458, 322-328, doi: 10.1038/nature07867.

Pambianco C., Colizza E., Melis R., Torricella F., Gallerani A., Miserocchi S. and Langone L.; 2025: *Past intrusion of circumpolar deep water in the Ross Sea: impacts on the ancient Ross Ice Shelf.* Science Advances, 11(26), eadt7075, doi:10.1126/sciadv.adt7075.

Pérez L.F., Martos Y.M., McKay R.M., De Santis L., Granot R., Bohaty S.M., Larter R. D., Williams T., Flores J. A., Olney M. T., Kulhanek D.K., Sauli C. and Gales J. A.; 2022: *Glacial to interglacial variations in the Ross Sea Embayment (Antarctica) during the late Neogene: insights from seismic stratigraphy and core-log-seismic integration.* Global and Planetary Change, 216, 103913, doi:10.1016/j.gloplacha.2022.103913.

Pollard D. and DeConto R.M.; 2009: *Modelling West Antarctic ice sheet growth and collapse through the past five million years*. Nature, 458, 329-332, doi: 10.1038/nature07809.

Prothro L.O., Simkins L.M., Majewski W. and Anderson J.B.; 2018: *Glacial retreat patterns and processes determined from integrated sedimentology and geomorphology records*. Mar. Geol., 395, 104-119, doi: 10.1016/j.margeo.2017.09.012.

Prothro L.O., Majewski W., Yokoyama Y., Simkins L.M., Anderson J.B., Yamane M., Miyairi Y. and Ohkouchi N.; 2020: *Timing and pathways of East Antarctic ice sheet retreat*. Quat. Sci. Rev., 230, 106166, doi: 10.1016/j.quascirev.2020.106166.

Quinn R., Bull J. and Dix J.; 1998: *Optimal processing of marine high resolution seismic reflection (Chirp) data*. Mar. Geophys. Res., 20, 13-20, doi: 10.1023/A:1004349805280.

Robinson D.E., Menzies J., Wellner J.S. and Clark R.W.; 2021: *Subglacial sediment deformation in the Ross Sea, Antarctica.* Quat. Sci. Adv., 4, 100029, doi: 10.1016/j.qsa.2021.100029.

Salvini F., Brancolini G., Busetti M., Storti F., Mazzarini F. and Coren F.; 1997: *Cenozoic geodynamics of the Ross Sea region, Antarctica: Crustal extension, intraplate strike-slip faulting, and tectonic inheritance*. J. Geophys. Res. Solid Earth, 102, 24669-24696, doi: 10.1029/97JB01643.

Sauli C., Busetti M., De Santis L. and Wardell N.; 2014: *Late Neogene geomorphological and glacial reconstruction of the northern Victoria Land coast, western Ross Sea (Antarctica)*. Mar. Geol., 355, 297-309, doi: 10.1016/j.margeo.2014.06.008.

Sauli C., Sorlien C., Busetti M., De Santis L., Geletti R., Wardell N. and Luyendyk B.P.; 2021: *Neogene development of the Terror Rift, western Ross Sea, Antarctica.* Geochemistry, Geophysics, Geosystems, 22(3), e2020GC009076, doi:10.1029/2020GC009076.

Schrader H. and Gersonde R.; 1978: *Diatoms and silicoflagellates*. In: Zachariasse W.J., Riedel W.R., Sanfilippo A., Schmidt R.R., Brolsma M.J., Schrader H.J., Gersonde R., Drooger M.M. and Broekman J.A. (eds), Micropaleontological counting methods and techniques: an exercise on an eight metres section of the lower Pliocene of Capo Rossello, Sicily, Utrecht Micropal. Bull., 17, pp. 129-176.

Simkins L.M., Anderson J.B., Greenwood S.L., Gonnermann H.M., Prothro L.O., Halberstadt A.R.W., Stearns L.A., Pollard D. and DeConto R.M.; 2017: *Anatomy of a meltwater drainage system beneath the ancestral East Antarctic ice sheet*. Nat. Geosci., 10, 691-697, doi: 10.1038/ngeo3012.

Smellie J.L. and Rocchi S.; 2021: *Chapter 5.1a Northern Victoria Land: volcanology*. In: Smellie J.L., Panter K.S. and Geyer A. (eds), Volcanism in Antarctica: 200 Million Years of Subduction, Rifting and Continental Break-up, Geological Society, London, Memoirs, pp. 347-381, doi: 10.1144/M55-2018-60.

Smith J.A., Graham A.G.C., Post A.L., Hillenbrand C.D., Bart P.J. and Ross D.P.; 2019: *The marine geological imprint of Antarctic ice shelves*. Nat. Commun., 10, 5635, doi: 10.1038/s41467-019-13496-5.

Shipp S., Anderson J. and Domack E.; 1999: *Late Pleistocene-Holocene retreat of the West Antarctic Ice Sheet system in the Ross Sea: Part 1 - Geophysical results.* Geol. Soc. Am. Bull., 111, 1486-1516.

Shipp S.S., Wellner J.S. and Anderson J.B.; 2002: *Retreat significance of a polar ice stream: sub-glacial geomorphic features and sediments from the Ross Sea, Antarctica*. In: Dowdeswell J.A. and O'Cofaigh C. (eds), Glacier-Influenced Sedimentation on High Latitude Continental Margins, Geological Society, London, Special Publications, 203, pp. 277-304.

Spector P., Stone J., Cowdery S.G., Hall B., Conway H. and Bromley G.; 2017: *Rapid early-Holocene deglaciation in the Ross Sea, Antarctica*. Geophys. Res. Lett., 44, 7817-7825, doi: 10.1002/2017GL074216.

Stuiver M. and Reimer P.J.; 1993: *Extended ^{14}C data base and revised CALIB 3.0 ^{14}C age calibration program.* Radiocarbon, 35(1), 215–230, doi:10.1017/S0033822200013904.

Stuiver M., Denton G.H., Hughes T.J. and Fastook J.L.; 1981: *History of the Antarctic Ice Sheet: success or failure?.* In: Denton G.H.and Hughes T.J. (eds), The Last Great Ice Sheets, John Wiley and Sons, New York, pp. 319–436.

Taviani M., Reid D. and Anderson J.; 1993: *Skeletal and isotopic composition and paleoclimatic significance of Late Pleistocene carbonates, Ross Sea, Antarctica*. J. Sediment. Res., 63, 84-90, doi: 10.1306/D4267A96-2B26-11D7-8648000102C1865D.

Tesi T., Belt S.T., Gariboldi K., Muschitiello F., Smik L., Finocchiaro F., Giglio F., Colizza E., Gazzurra G., Giordano P., Morigi C., Capotondi L., Nogarotto A., Köseoglu D., Di Roberto A., Gallerani A. and Langone L.; 2020: *Resolving sea ice dynamics in the north-western Ross Sea during the last 2.6 ka: from season to millennial timescales.* Quat. Sci. Rev., 237, 106299, doi: 10.1016/j.quascirev.2020.106299.

Torricella F., Melis R., Malinverno E., Fontolan G., Bussi M., Capotondi L., Del Carlo P., Di Roberto A., Geniram A., Kuhn G., Khim B.-K., Morigi C., Scateni B. and Colizza E.; 2021: *Environmental and oceanographic conditions at the continental margin of the Central Basin, northwestern Ross Sea (Antarctica) since the Last Glacial Maximum*. Geosciences, 11, 155, doi: 10.3390/geosciences11040155.

Warnock J.P. and Scherer R.P.; 2014: *A revised method for determining the absolute abundance of diatoms.* Journal of Paleolimnology, 53(1), 157–163, doi:10.1007/s10933-014-9813-1.

Wentworth C.K.; 1922: *A scale of grade and class terms for clastic sediments*. J. Geol., 30, 377-392.

Yokoyama Y., Anderson J.B., Yamane M., Simkins L.M., Miyairi Y., Yamazaki T., Koizumi M., Suga H., Kusahara K., Prothro L., Hasumi H., Southon J.R. and Ohkouchi N.; 2016: *Widespread collapse of the Ross ice shelf during the late Holocene.* Proceedings of the National Academy of Sciences of the USA, 113, 2354-2359, doi: 10.1073/pnas.1516908113.

Zhu J., Wei Y., Li H. and Ma J.; 2016: *Chirp sub-bottom profiler signal processing method based on fractional Fourier transform*. In: 2016 IEEE/OES China Ocean Acoustics (COA 2016), Harbin, China, 9-11 January 2016, doi: 10.1109/COA.2016.7535708.

Corresponding author: Chiara Sauli
National Institute of Oceanography and Applied Geophysics – OGS
Borgo Grotta Gigante, 42/c - 34010 Sgonico, Trieste, Italy
Phone: +39 0402140; e-mail: csauli@ogs.it

Appendix: Radiocarbon dating

The chronology of the GC01 and GC02 cores is based on eight accelerator mass spectrometry (AMS) radiocarbon dates performed at the Dating and Diagnostics Centre of the University of Salento (Italy). Seven radiocarbon analyses were carried out on mixed calcareous benthic foraminifera and one analysis was made using acid insoluble organic matter (AIOM). Three unpublished additional dating analyses, performed at the Poznan Radiocarbon Laboratory, Adam

Mickiewicz University (Poland) and at the NOSAMS Woods Hole Oceanographic Institution (USA) on foraminifera and on AIOM, from selected levels of the NW02 core, were used for this work (Table A1).

The dates obtained from carbonate matrix were directly calibrated, while the dates obtained from AIOM matrix were processed before the calibration into ^{14}C ages. Radiocarbon chronologies utilising the AIOM fraction from bulk sediments are frequently undermined by contamination from reworked ancient organic carbon resulting from glacial erosion and/or the disturbance of unconsolidated sediments. The AIOM dates of Antarctic surface sediments demonstrate a temporal range spanning several thousand years (Andrews *et al*., 1999; Mezgec *et al*., 2017; Prothro *et al*., 2020; Ha *et al*., 2023).

Table A1 - The table provides information on: a) the morphobathymetric, b) the acoustic (chirp and sparker), and c) single-channel seismic (SCS) and multichannel seismic (MCS) data presented in the paper.

Project	Data	Instrument
GLEVORS Project 32nd PNRA Cruise 2016–17	Multibeam data	Multibeam echo sounder SeaBat 8111 system, 100 kHz
VILD Project 21st PNRA Cruise 2005–06	Multibeam data	Multibeam echo sounder Reson 8111 hull-mounted, processed using Teledyne Reson PDS2000 and Teledyne CARIS software
NBP9801 Nathaniel B. Palmer Cruise 1998	Multibeam data	Multibeam swath mapping sonar SB2112 system, 12 kHz
GLEVORS Project 32ndPNRA Cruise 2016–17	Sub-bottom profiler data (592 profiles)	Benthos Chirp III, 2-7 kHz Array of 4×4 transducers
14th PNRA Cruise 1998–99	(0.2–1kJ) Sparker (multi-array 150 dip)	0.4–2.5 kHz dominant frequency
GLEVORS Project 32nd PNRA Cruise 2016–17	SCS	2×210 in3 GI gun 105G+105I harmonic gun mod 10-element single-channel streamer Sampling rate 1 ms
VILD Project 17th PNRA Cruise 2001–02	SCS	Single GI gun of 105 in3 (for 210 in3 in harmonic) and of 250 in3 (for 355 in3 harmonic), Operating pressure 140 bar (2000 psi) Depth 6 m - Streamer length 15 m Record length 4 s - Sampling rate 2000 Hz
6thPNRA Cruise 1990–91	30-fold MCS	2×20 guns – capacity 74.8 l Depth 6 m - Shot interval 50 m Streamer length 3000 m Channels 120 at 12 m deep Record length 10 s - Sampling rate 2 ms

Before calibration, all the AIOM dates were corrected by subtracting 3.8 ka which represents the local contamination with older organic matter calculated by Andrews *et al*. (1999) for this latitude in the Ross Sea, and if this contamination has not changed during the last 30 ka (Hall *et al*., 2010; Mezgec *et al*., 2017, Prothro *et al*., 2020).

The corrected AMS ^{14}C dates performed on AIOM and the dates on foraminifera tests were converted into calibrated ages by means of Calib8.2 (Stuiver and Reimer, 1993) at 95% confidence ranges. The MARINE20 calibration curve (Heaton *et al*., 2020), assuming regional marine offset (ΔR) 609 ± 137 years from the global marine reservoir effect following the values calculated for

the Ross Sea area by Gao *et al*. (2022), was used for ages younger than 11 ka, while the glacial scenario (GS) adjustment to the Δ*R* proposed by Heaton *et al*. (2023) was used for dates older than 11 ka in order to account for changes in the ^{14}C depletion, predominantly driven by the increased sea-ice coverage within polar oceans following the instauration of a glacial period. This resulted in a ΔR_{GS} of 1069 ± 137 years, corresponding to the Holocene Δ*R* with the addition of 460 years as recommended by Heaton *et al*. (2023) for these latitudes.

New uncorrected and calibrated ^{14}C data are summarised in Table A2 uncorrected dating coming from published papers by Licht *et al*. (1996, 1999), Melis *et al*. (2002), and Colizza *et al*. (2003) was also used to uniformly recalibrate all ages (Table A1). All the ages reported in this paper represent the calibrated ages unless otherwise specified.

Table A2 - The table shows the conventional and corrected radiocarbon ages for the studied samples with an indication of the absolute error of the measurement. The radiocarbon ages were converted into calibrated ages by means of Calib8.2 (Stuiver and Reimer, 1993) at 95% confidence ranges. Row ages of cores DF80-144 and DF87-32 have been recalibrated from Licht *et al.* (1996).

Core	Laboratory code	Sample depth (cm)	Carbon source	Conventional ^{14}C age (yrs BP)	Age error	AIOM corrected (- 3.8 A*)	Median cal age (yrs BP)
IT17 RS-01	LTL18457A	0-1	forams	2635	45		1436
IT17 RS-02	LTL18452A	0-1	forams	1759	45		571
IT17 RS-02	LTL18453A	5-6	forams	1801	45		608
IT17 RS-02	LTL18454A	10-11	forams	2306	45		1088
IT17 RS-02	LTL18455A	19-20	forams	3344	45		2279
IT17 RS-02	LTL18456A	25-26	forams	4370	45		3534
IT17 RS-02	LTL20157A	35-36	AIOM	22267	120	18467	20104
ANTA99_27	GX-28119	71-72	AIOM	27640	260	23840	26146
ANTA99_27	GX-28120	231-232	AIOM	31560	400	27760	30600
ANTA99_31	GX-28121	41-42	AIOM	8800	50	5000	4347
ANTA99_31	GX-28122	91-92	AIOM	25290	190	21490	24115
ANTA99_31	GX-28123	217-218	AIOM	30380	340	26580	29353
ANTA02-NW2	OS- 62326	top	mixed forams	1270	60		168
ANTA02-NW2	Poz-141026	32-33	benthic forams	17700	100		19171
ANTA02-NW2	OS- 61612	158-159	AIOM	24100	120	20300	22316
DF80-144	CAMS 11798	8-11	AIOM	6330	80	2530	1324
DF80-144	AA 12899	13-14	forams	21255	200		23342
DF80-144	CAMS 12582	21-24	AIOM	22360	140	18560	20214
DF80-144	AA 17399	200	forams	32685	610		35240
DF87-32	CAMS 4062	18-20	AIOM	23390	240	19590	21486
DF87-32	AA 9361	80-84.5	mixed carb	27720	340		30021

* in agreement with Andrews *et al.* (1999)